

# Geometry of dynamics and phase transitions in classical lattice $\varphi^4$ theories

Lando Caiani<sup>1,a</sup>, Lapo Casetti<sup>2,3,b</sup>, Cecilia Clementi<sup>1,c</sup>,  
Giulio Pettini<sup>4,d</sup>, Marco Pettini<sup>5,e</sup> and Raoul Gatto<sup>3,f</sup>

<sup>1</sup>*International School for Advanced Studies (ISAS/SISSA), via Beirut 2-4, I-34014 Trieste, Italy*

<sup>2</sup>*Scuola Normale Superiore, Piazza dei Cavalieri 7, I-56126 Pisa, Italy*

<sup>3</sup>*Département de Physique Théorique, Université de Genève, 24 Quai Ernest-Ansermet, CH-1211 Genève, Switzerland*

<sup>4</sup>*Dipartimento di Fisica, Università di Firenze, Largo E. Fermi 2, I-50125 Firenze, Italy*

<sup>5</sup>*Osservatorio Astrofisico di Arcetri, Largo E. Fermi 5, I-50125 Firenze, Italy*

(October 21, 2018)

## Abstract

We perform a microcanonical study of classical lattice  $\varphi^4$  field models in 3 dimensions with  $O(n)$  symmetries. The Hamiltonian flows associated to these systems that undergo a second order phase transition in the thermodynamic limit are here investigated. The microscopic Hamiltonian dynamics neatly reveals the presence of a phase transition through the time averages of conventional thermodynamical observables. Moreover, peculiar behaviors of the largest Lyapounov exponents at the transition point are observed. A Riemannian geometrization of Hamiltonian dynamics is then used to introduce other relevant observables, that are measured as functions of both energy density and temperature. On the basis of a simple and abstract geometric model, we suggest that the apparently singular behaviour of these geometric observables might probe a major topological change of the manifolds whose geodesics are

the natural motions.

PACS numbers(s): 05.20.-y; 05.45.+b; 02.40.-k

## I. INTRODUCTION

The general problem of the relevance of microscopic dynamics to the statistical behaviour of physical systems dates back to Boltzmann's ideas at the very beginning of statistical mechanics, and is still far from being clarified and solved. Within this framework, one can extract a less general but still challenging question, i.e. whether the microscopic Hamiltonian dynamics displays some relevant change when a given system undergoes a phase transition.

Studying microscopic Hamiltonian dynamics means that – instead of using *ensemble* statistical averages – one numerically computes *time* averages of the relevant observables. There are two main reasons for so doing: *i)* there exist interesting observables that are intrinsically dynamical, as is the case of Lyapounov exponents; *ii)* through a differential-geometric description of the dynamics, based on simple tools of Riemannian geometry, new concepts and methods come to enrich the standard approaches to the study of phase transitions, hinting to a possibly deeper characterization of their very nature from the standpoint of the mathematical structures involved.

The geometric formulation of the dynamics of many-degrees-of-freedom systems was first used by Krylov in his pioneering studies on the dynamical foundations of statistical mechanics [1]. Then, during the last two decades, there have been some attempts to cope with the ergodicity of Hamiltonian systems through a geometric theory of dynamics [2]. A more recent series of papers [3–8], instead of dealing with ergodicity, successfully addresses the problem of explaining and quantifying Hamiltonian chaos within a geometric framework where natural motions are seen as geodesics of a suitable Riemannian manifold (henceforth referred to as “mechanical manifold”). Here chaotic dynamics stems from curvature fluctuations along the geodesics, through a mechanism similar to the parametric destabilization of the stable orbits of a pendulum. At variance with a widespread belief, negative curvatures do not appear essential to produce chaos, positive and fluctuating curvatures can work as well. A very interesting point is that the average degree of instability of the dynamics is given in terms of curvature-related quantities integrated over the whole “mechanical

manifold”. This establishes a link between a *dynamical* aspect of a given system — the stability/instability of its trajectories — and some *global geometric* properties of its associated “mechanical manifold”.

Now, when a model system displays a phase transition, a natural question arises: what kind of relationship exists – if any – between all the well-known major thermodynamic changes occurring at the transition point and the mentioned global geometric characteristics of the “mechanical manifolds”? The present work actually shows that a second order phase transition appears to be associated with an abrupt change in the global geometry — and possibly in the topology, as we conjecture — of the “mechanical manifolds”.

The above problematics is addressed in the present work by studying the dynamics of classical field theories, discretized on a lattice. A classical lattice field theory can be regarded as a discrete classical dynamical system. In particular, we shall consider the classical  $\varphi^4$  theory, whose lattice version is a set of coupled nonlinear oscillators.

Equilibrium phase transitions are usually studied in the framework of the Gibbsian canonical ensemble. Dynamics, when it is considered, is introduced only *a posteriori*: the most common procedure is to describe it by means of non-deterministic equations, usually of the Langevin type, whose limiting probability distribution is the Boltzmann weight  $\exp(-H/T)$  where  $H$  is the Hamiltonian of the system. Here we are going to adopt a completely different approach, i.e. from the very beginning we consider the deterministic Hamiltonian dynamics, without making explicit assumptions on the equilibrium properties of the system, and we observe how the phase transition is signaled by the dynamics. On rigorous grounds, one cannot be sure that a phase transition does exist in a system studied through its Hamiltonian dynamics, because there is no proof of the fact that the dynamics is ergodic. Moreover, even assuming that it is ergodic, the ergodic measure will be the microcanonical rather than the canonical one. The two ensembles are equivalent only in the thermodynamic limit, thus the phenomenology observed in finite systems, as the systems considered in numerical simulations necessarily are, might be different. To give only an example, let us consider the phenomenon of *ergodicity breaking*, i.e. the fact that ergodicity

is not valid for the whole phase space but only for disjoint subsets of it. Such a phenomenon is indeed tightly related to phase transitions; in fact, when it occurs it entails a symmetry breaking, as in usual phase transitions. But ergodicity breaking is a more general concept than symmetry breaking, in fact it is also at the origin of those phase transitions which do not correspond to the breaking of an evident symmetry of the Hamiltonian (for example in spin glasses) [9–11]. In the canonical ensemble, ergodicity can be broken only in the thermodynamic limit [12], while in the microcanonical ensemble, in principle, there might be ergodicity breaking also in finite systems. Ergodicity being a dynamical property, we think that a dynamical approach is particularly appropriate to study such a phenomenon.

It is worth mentioning here that ergodicity breaking in classical Hamiltonian systems can be related with supersymmetry breaking [13]; this relation is established within the framework of a path-integral formulation of classical mechanics, where the bosonic sector of a supersymmetric Lagrangian is given by a suitable function of the canonical coordinates, obeying standard Hamilton equations, and the fermionic sector contains ghost fields that - rather surprisingly - obey the Jacobi equation describing the stability of classical paths [14,15]. In this framework the spontaneous symmetry breaking can occur also at finite volume [13].

Our results show that, as far as the lattice  $\varphi^4$  models considered are concerned, the numerical phenomenology, obtained by simulating Hamiltonian dynamics, is perfectly consistent with the expectations based on equilibrium statistical mechanics. Moreover, we investigate whether the instability of dynamical trajectories, measured by Lyapounov exponents, is sensitive to the phenomenon of phase transition [16]. In the light of the geometrization of dynamics, Lyapounov exponents are also seen as probes of the hidden geometry of motion, and in fact our results suggest that the deep origin of ergodicity breaking and of the dynamical counterpart of a phase transition could be found in a major change in the geometric – or even topologic – structure of the “mechanical manifolds” underlying the dynamics.

The paper is organized as follows: in Section II we introduce the models studied, we describe the numerical techniques which we adopted, and we discuss the phenomenology of

the phase transition as it emerges from the dynamics. In Section III the main definitions and results of the Riemannian description of Hamiltonian chaos are given, and the behaviour of the geometric observables in our models is presented and discussed together with an interpretation involving simple topological concepts. Section IV is devoted to some remarks and comments.

## II. MODELS AND NUMERICAL RESULTS

To study the relationship between microscopic dynamics and equilibrium phase transitions we consider Hamiltonian systems of the standard type

$$H[\varphi, \pi] = \frac{1}{2} \sum_{\mathbf{i}} \pi_{\mathbf{i}}^2 + V(\{\varphi_{\mathbf{i}}\}) , \quad (1)$$

where  $\varphi_{\mathbf{i}}$  and  $\pi_{\mathbf{i}}$  are canonically conjugated coordinates and momenta,  $\mathbf{i}$  labels the sites of a  $d$ -dimensional cubic lattice, and  $V$  is an interaction potential.

More precisely, we consider models which can be derived from the paradigm Hamiltonian

$$H[\varphi] = \int d^d x \left\{ \frac{1}{2} \pi^2(\mathbf{x}) + J \frac{1}{2} [\nabla_d \varphi(\mathbf{x})]^2 - \frac{1}{2} \varphi^2(\mathbf{x}) + \frac{\lambda}{4} \varphi^4(\mathbf{x}) \right\} . \quad (2)$$

where  $\pi(\mathbf{x}) = \delta L[\varphi, \dot{\varphi}] / \delta \dot{\varphi}(\mathbf{x}) = \dot{\varphi}(\mathbf{x})$  is the canonically conjugated momentum density of  $\varphi(\mathbf{x})$ , by discretizing it on a lattice. By means of the following substitutions

$$\partial_{\mu} \varphi(\mathbf{x}) \rightarrow \frac{\varphi(\mathbf{x} + a \mathbf{e}_{\mu}) - \varphi(\mathbf{x})}{a} , \quad (3)$$

$$\int d^d x \rightarrow a^d \sum_{\mathbf{i}} ,$$

we obtain

$$H[\varphi, \pi] = a^d \sum_{\mathbf{i}} \left[ \frac{1}{2} \pi_{\mathbf{i}}^2 + \frac{J}{2a^2} \sum_{\mu=1}^d (\varphi_{\mathbf{i}+\mathbf{e}_{\mu}} - \varphi_{\mathbf{i}})^2 - \frac{1}{2} m^2 \varphi_{\mathbf{i}}^2 + \frac{\lambda}{4} \varphi_{\mathbf{i}}^4 \right] . \quad (4)$$

where  $a$  is the lattice spacing,  $\mathbf{e}_{\mu}$  is the unit vector in the  $\mu$ -th direction of the lattice and  $\varphi_{\mathbf{i}} = \varphi(\mathbf{x}_{\mathbf{i}})$ . This system shows (at equilibrium) a continuous phase transition with nonzero

critical temperature corresponding to a spontaneous breaking of the discrete  $O(1)$  — or  $\mathbb{Z}_2$  — symmetry.

We have also considered the vector versions of this lattice  $\varphi^4$  model described by the Hamiltonian

$$H[\varphi, \pi] = a^d \sum_{\alpha} \sum_{\mathbf{i}} \left[ \frac{1}{2} (\pi_{\mathbf{i}}^{\alpha})^2 + \frac{J}{2a^2} \sum_{\mu=1}^d (\varphi_{\mathbf{i}+\mathbf{e}_{\mu}}^{\alpha} - \varphi_{\mathbf{i}}^{\alpha})^2 - \frac{1}{2} m^2 (\varphi_{\mathbf{i}}^{\alpha})^2 \right] + \frac{\lambda}{4} \sum_{\mathbf{i}} \left[ \sum_{\alpha} (\varphi_{\mathbf{i}}^{\alpha})^2 \right]^2. \quad (5)$$

where the index  $\alpha$  runs from 1 to  $n$ . We have considered, in addition to  $n = 1$ ,  $n = 2$ , which is the simplest vector case, and  $n = 4$ , which is the largest value of  $n$  that allowed for a complete numerical study with our computing resources. For  $n > 1$  the broken symmetry is a continuous one (the potentials are respectively invariant under planar rotations,  $O(2)$ , and under the action of the  $O(4)$  group). Because of the Mermin-Wagner theorem, the interactions being of short range, the  $O(2)$  and  $O(4)$  models can have a second order phase transition only on three dimensional lattices.

The Hamiltonian dynamics — and thus the related dynamical, thermodynamical and geometrical quantities — is studied by molecular dynamics simulations performed at several values of the energy density  $\varepsilon = E/N$ , which is the relevant physical parameter as long as our systems are in a microcanonical ensemble<sup>1</sup>.

## A. Numerical study of dynamics and thermodynamics

The canonical equations of motion

$$\dot{\varphi}_{\mathbf{i}}^{\alpha} = \frac{\partial H}{\partial \pi_{\mathbf{i}}^{\alpha}} \quad (6)$$

$$\dot{\pi}_{\mathbf{i}}^{\alpha} = -\frac{\partial H}{\partial \varphi_{\mathbf{i}}^{\alpha}} \quad (7)$$

---

<sup>1</sup>The qualitative features of the results are not affected if we consider the temperature (average kinetic energy per degree of freedom) as the physical parameter.

yield

$$\begin{aligned}\dot{\varphi}_{\mathbf{i}}^{\alpha} &= \pi_{\mathbf{i}}^{\alpha} \\ \dot{\pi}_{\mathbf{i}}^{\alpha} &= A \sum_{\mu=1}^d (\varphi_{\mathbf{i}+\mathbf{e}_{\mu}}^{\alpha} + \varphi_{\mathbf{i}-\mathbf{e}_{\mu}}^{\alpha}) + B\varphi_{\mathbf{i}}^{\alpha} - C\|\varphi_{\mathbf{i}}^{\alpha}\|^2\varphi_{\mathbf{i}}^{\alpha} \quad ,\end{aligned}\tag{8}$$

with

$$\begin{aligned}A &= Ja^{d-2} \\ B &= m^2a^d - 2Ja^{d-2}d \\ C &= \lambda a^d \quad ,\end{aligned}\tag{9}$$

and  $\|\varphi_{\mathbf{i}}^{\alpha}\|^2 = \sum_{\alpha}(\varphi_{\mathbf{i}}^{\alpha})^2$ . In order to guarantee a faithful numerical representation of a Hamiltonian flow, it is necessary that the algorithm updates the canonical coordinates,  $[\varphi_{\mathbf{i}}^{\alpha}(n\Delta t), (\pi_{\mathbf{i}}^{\alpha}(n\Delta t))] \rightarrow [\varphi_{\mathbf{i}}^{\alpha}((n+1)\Delta t), (\pi_{\mathbf{i}}^{\alpha}((n+1)\Delta t))]$ , by means of a canonical, i.e. symplectic, transform. Symplectic algorithms ensure the conservation of Poincaré geometric invariants, and, in particular, of phase space volumes and energy conservation. We used a very efficient and precise third order symplectic algorithm recently proposed [17], keeping the fluctuations of relative energy at  $\Delta E/E \simeq 10^{-9}$ . All the simulations have been performed using words of 64 bits. We have always chosen random initial conditions at equipartition among momenta in order to consider phase space trajectories stemming from initial conditions that belong to the support of an equilibrium measure.

Along the phase space trajectories — worked out numerically — the time averages of any observable  $A$  is computed as

$$\overline{A}^t = \frac{1}{t} \int_0^t d\tau A[\pi(\tau), \varphi(\tau)] \quad .\tag{10}$$

By means of such averages both dynamical and thermodynamical properties of the system under investigation can be determined.

One of the most relevant properties of the dynamics is its degree of instability, because it is related to the efficiency of phase mixing. Let us remember that the the strength of



dynamical instability, i.e. of *chaos*, is measured by the largest Lyapounov exponent  $\lambda_1$ . If we denote by  $\mathcal{M}$  the phase space of the system and by  $X$  a vector field on it, such that

$$\dot{x}^i = X^i(x^1 \dots x^N) \quad (11)$$

are the equations of motion, a complete integral of this dynamical system defines a one-parameter group of diffeomorphisms of  $\mathcal{M}$ , that is  $\phi^t : \mathcal{M} \rightarrow \mathcal{M}$ . Denote by

$$\dot{\xi}^i = \mathcal{J}_k^i[x(t)] \xi^k \quad (12)$$

the tangent dynamics equation, i.e. the realization of the mapping  $d\phi^t : T_x\mathcal{M} \rightarrow T_{\phi^t(x)}\mathcal{M}$ , where  $[\mathcal{J}_k^i]$  is the Jacobian matrix of  $[X^i]$ , then the largest Lyapounov exponent  $\lambda_1$  is defined by

$$\lambda_1 = \lim_{t \rightarrow \infty} \frac{1}{t} \ln \frac{\|\xi(t)\|}{\|\xi(0)\|} \quad (13)$$

and, by setting  $\Lambda[x(t), \xi(t)] = \xi^T \mathcal{J}[x(t)] \xi / \xi^T \xi \equiv \xi^T \dot{\xi} / \xi^T \xi = \frac{1}{2} \frac{d}{dt} \ln(\xi^T \xi)$ , this can be formally expressed as a time average

$$\lambda_1 = \lim_{t \rightarrow \infty} \frac{1}{2t} \int_0^t d\tau \Lambda[x(\tau), \xi(\tau)] \quad (14)$$

In practice, as we deal with standard Hamiltonians, the tangent dynamics (12) can be written in the form

$$\frac{d^2 \xi_q^i}{dt^2} + \left( \frac{\partial^2 V}{\partial \varphi_i \partial \varphi^j} \right)_{\varphi(t)} \xi_q^j = 0 \quad (15)$$

which, integrated along any numerical trajectory of Eqs.(8), makes possible the estimate of  $\lambda_1$  from

$$\lambda_1(t_{\mathcal{N}}) = \frac{1}{\mathcal{N} \Delta t} \sum_{n=1}^{\mathcal{N}} \ln \left( \frac{\|\xi(t_n)\|}{\|\xi(t_{n-1})\|} \right) \quad (16)$$

where  $\{\xi^i\} = (\{\xi_q^i\}, \{\xi_p^i\})$ ,  $\xi_p^i(t) = [\xi_q^i(t + \Delta t) - \xi_q^i(t - \Delta t)]/2\Delta t$ , and  $t_n = n\Delta t$  ( $\Delta t$  is some time interval). The average is extended up to a final time  $t_{\mathcal{N}}$  such that  $\lambda_1(t_{\mathcal{N}})$  has attained a *bona fide* asymptotic value.

For what concerns thermodynamic observables, temperature — the basic quantity — is determined through the time average of kinetic energy per degree of freedom

$$\frac{1}{2}T = \frac{1}{t} \int_0^t d\tau \left\{ \frac{1}{Nn} \sum_{\alpha, \mathbf{i}} \frac{1}{2} [\pi_{\mathbf{i}}^{\alpha}(\tau)]^2 \right\} \quad (17)$$

where  $N$  is the number of lattice sites and  $t$  is the total time during which a phase space trajectory is followed. This quantity shows a fast convergence in time and is expected to differ from its canonical counterpart by a  $\mathcal{O}(\frac{1}{Nn})$  correction.

Besides the bifurcation of the order parameter —  $\langle \varphi \rangle$  — at some critical value of the temperature, a second order phase transition is signaled by a singular temperature dependence of the specific heat, and therefore the microcanonical computation of the constant volume specific heat  $C_V$  deserves special care. An efficient numerical method to compute  $C_V$  is devised by inverting a general formula relating canonical and microcanonical averages of the squared fluctuations of a generic observable [19] by applying it to the fluctuations of kinetic energy

$$\overline{\delta K^2} = \widehat{\delta K^2} - \frac{\beta^2}{C_V} \left( \frac{\partial \widehat{K}}{\partial \beta} \right)^2, \quad (18)$$

where  $C_V = (\partial E / \partial T)$ ; overbar and hat stand for microcanonical and canonical averages respectively.

The quantity  $\overline{\delta K^2}$  can be easily computed along the numerical trajectories, whereas the analytic expressions  $\bar{K} = \widehat{K} = N/2\beta$ ,  $\widehat{\delta K^2} = N/(2\beta^2)$  are readily found. By inverting the equation above one immediately finds a formula for a microcanonical estimate of the canonical specific heat

$$C_V = \frac{Nn}{2} \frac{1}{1 - (Nn/2)[(\overline{\delta K^2})/(\bar{K}^2)]} \quad (19)$$

which requires the numerical computation of time averages of kinetic energy and of its squared fluctuations;  $Nn$  is the total number of degrees of freedom.

## B. Dynamical evidence of the phase transition

### 1. Detecting the transition: Binder cumulants

In the canonical ensemble, a phase transition may show up only in the thermodynamic limit. As long as  $N$  is finite, all the thermodynamic quantities are regular functions of the temperature, and ergodicity and symmetry are not broken. Nevertheless, some marks of the transition show up neatly also in a finite system. The specific heat does not diverge, but exhibits a peak — whose height grows with the size of the system — at a temperature  $T_c^{Cv}(N)$ . In principle the order parameter is expected to vanish on the whole temperature range for any finite value of  $N$ , though in practice, e.g., in a canonical MonteCarlo simulation where the length of the sampling of  $\varphi$  is necessarily finite, the system is trapped in one of the two phases for a “time” which grows exponentially with  $N$  [9], and thus a fictitious symmetry breaking is observed at a temperature  $T_c^\varphi(N)$ . This temperature, in general, does not coincide with  $T_c^{Cv}(N)$ , even if

$$\lim_{N \rightarrow \infty} T_c^{Cv}(N) = \lim_{N \rightarrow \infty} T_c^\varphi(N) = T_c^\infty . \quad (20)$$

In the microcanonical ensemble ergodicity breaking may occur also at finite  $N$ , hence we can expect that a “true” critical energy exists also at finite  $N$ . No rigorous theoretical result is at our disposal regarding this aspect. Nevertheless, on the basis of asymptotic equivalence of statistical ensembles, the behaviour of microcanonical thermodynamic functions is reasonably expected to be similar to the canonical case, at least as  $N$  is sufficiently large. Indeed this is what is observed, as we shall see in the following. In particular, we expect the specific heat to exhibit a peak at a critical energy density which is a function of  $N$ .

In the framework of the statistical theory of critical phenomena, by means of the finite-size scaling analysis [22,21] the critical properties of the infinite system are inferred from the values of the thermodynamic observables in finite samples of different sizes. In particular it is possible to locate the critical point by means of the so-called *Binder cumulants* [22]. The Binder cumulant  $g$  that we have computed for our systems is defined as

$$g = 1 - \frac{\langle \varphi^4 \rangle}{3 \langle \varphi^2 \rangle^2} , \quad (21)$$

where

$$\begin{aligned}\langle \varphi^{2n} \rangle &= \left\langle \left( \sum_{\alpha} \langle \varphi \rangle_{\alpha}^2 \right)^n \right\rangle \\ \langle \varphi \rangle_{\alpha} &= \sum_{\mathbf{i}} \varphi_{\mathbf{i}}^{\alpha} \quad .\end{aligned}$$

In the disordered phase the probability distribution of the order parameter will be nearly Gaussian with zero mean, hence  $g \simeq 0$ . At variance to this, at zero temperature (or energy), when  $\varphi_i \equiv \varphi_0$  with no fluctuations,  $g = 2/3$ . At different sizes of the system,  $g$  will decay following different patterns  $g(N, T)$  from  $2/3$  to  $0$  at increasing temperature. The remarkable fact is that the value of  $g$  at  $T_c^{\infty}$  is *independent* of  $N$ , provided  $N$  is large enough for the scaling regime to set in; hence the critical point can be located by simply looking at the intersection of the different curves  $g(N, T)$  for different values of  $N$ . In principle, two different sizes are sufficient to locate the transitions; in practice, owing to the unavoidable numerical errors which affect  $g$ , it is necessary to consider at least three values of  $N$ . Moreover, the value of  $g$  at the critical point, usually referred to as  $g^*$ , is a universal quantity, like the critical exponents; for a simple proof see e.g. Ref. [21]. The importance of the Binder cumulant method is not only that it allows to easily locate the critical temperature, without the need of an extrapolation of the asymptotic behaviour of the fictitious finite- $N$  critical temperatures, but also that such an estimate of  $T_c^{\infty}$  is independent of the other thermodynamic observables like  $\langle \varphi \rangle$  or  $C_V$ , and this is obviously a great advantage in determining the actual critical behaviour — in particular the critical exponents. Moreover, one can regard the existence of a crossing of different curves  $g(N, T)$  as a “proof” for the existence of a phase transition in the system under investigation. This may be useful in various cases where the presence of singularities in the thermodynamic functions or the existence of a nonzero order parameter are difficult to observe (e.g. this is the case of spin glasses [23]).

The theory behind the Binder cumulant method is totally internal to *canonical* statistical mechanics: to our knowledge no extension of this theory to the *microcanonical* ensemble exists. Nevertheless we will adopt the pragmatic point of view of assuming its validity as a numerical tool also in our dynamical simulations, and our operative definition of the critical

energy density  $\varepsilon_c^\infty$  will be the intersection point of the curves  $g(N, \varepsilon)$  at different  $N$ . The consistency of the method will be checked *a posteriori*. In the following, unless explicitly stated otherwise,  $\varepsilon_c$  and  $T_c$  will denote respectively  $\varepsilon_c^\infty$  and  $T_c^\infty$ .

The results for  $g(N, \varepsilon)$  at different sizes for the  $\varphi^4$  lattice models are shown in Figs.1*a, b, c*. The crossing of the various curves at  $\varepsilon_c \simeq 31$  for the  $O(1)$  model is quite evident, and similarly at  $\varepsilon_c \simeq 44$  for the  $O(2)$  model, and at  $\varepsilon_c \simeq 56$  for the  $O(4)$  model.

Such estimates of the critical energy densities are obviously far from being extremely accurate. However, we are mainly interested in showing that the dynamical phenomenology is actually consistent with the existence of an equilibrium phase transition at finite energy density, and the values of  $\varepsilon_c$  are needed to understand whether or not the singular (or, more generally, peculiar) behaviours of the observables — either thermodynamical, or strictly dynamical, or geometric ones — that we are going to study can be associated with the phase transition.

## 2. Temperature

The temperature of the  $\varphi^4$  systems, numerically determined according to Eq. (17), is plotted in Fig.2 as a function of the energy density  $\varepsilon$ . Note that for all the models a change of the function  $T(\varepsilon)$  is clearly evident at  $\varepsilon = \varepsilon_c$ .

By plotting the Binder cumulants *vs.* the temperature  $T$ , the critical values  $T_c$  are obtained for all the models and are found in complete agreement with the outcomes of the  $T(\varepsilon)$  curves. These values are:  $T_c \simeq 35$  for the  $O(1)$  model,  $T_c \simeq 25$  for the  $O(2)$  model, and  $T_c \simeq 16$  for the  $O(4)$  model.

## 3. Specific heat

The specific heat  $c_V = C_V/Nn$  per degree of freedom of the  $\varphi^4$  models here considered, computed according to Eq. (19), is plotted *vs.* the temperature in Fig.3. The asymptotic values of the specific heat in the limits  $T \rightarrow 0$  and  $T \rightarrow \infty$  are exactly known. In fact at

low energies the anharmonic terms in the Hamiltonian can be neglected, thus the system behaves as a collection of harmonic oscillators and  $c_V \rightarrow 1$  as  $T \rightarrow 0$ . In the high-energy limit the quadratic terms in the potential are negligible with respect to the quartic ones, whence  $c_V \rightarrow 1/2 + 1/4 = 3/4$  as  $T \rightarrow \infty$ . At intermediate energy densities, neat peaks show up whose positions are close to  $T_c$  for each model respectively. The heights of the peaks are found to grow with  $N$  and to decrease with  $n$ .

#### *4. Dynamical properties*

We have shown that the outcomes of the dynamical numerical simulations of the scalar and vector versions of the lattice  $\varphi^4$  model are perfectly consistent with the expectations of the effects of a second order phase transition on a finite sample. As already motivated above, this first result is non-trivial. Up to now its content is that — for all practical purposes — a dynamical simulation is actually equivalent to a microcanonical one, so that, at sufficiently large  $N$ , the results are in natural agreement with canonical statistical mechanics. All these results concern time averages: the time variable, even if not eliminated from the very beginning as in the statistical approach, has been nonetheless integrated out in the averaging procedure. But we can also wonder what are the properties — if any — that are peculiar to the dynamics and that can be considered relevant to the description of the phase transition itself. Moreover we have already noticed that the phenomenon of ergodicity breaking has a deep dynamical origin, therefore we can try to understand what features are associated to a Hamiltonian ergodicity breaking.

The lattice  $\varphi^4$  models under investigation are nonintegrable dynamical systems. In the two limits  $\varepsilon \rightarrow 0$  and  $\varepsilon \rightarrow \infty$ , these systems become integrable. The two integrable limits are respectively those of a system of coupled harmonic oscillators and of a system of independent quartic oscillators. The dynamics is always chaotic over the whole energy range. Nevertheless, in analogy to other nonlinear oscillator systems, by varying the energy we expect that qualitatively different dynamical regimes will be found, characterized by a tran-

sition between different behaviours of the largest Lyapounov exponent  $\lambda_1$  as a function of energy density or, equivalently, temperature. This phenomenon is attributed to a dynamical transition between weak and strong chaos, it is known as Strong Stochasticity Threshold (SST) and is discussed in refs. [24,25]. In particular, the following questions naturally arise. Is there any peculiar behaviour of the Lyapounov exponent in correspondence with the phase transition? Is there a transition between strongly and weakly chaotic regimes also in these models, and, in the affirmative case, is there any relationship between these different dynamical regimes and the thermodynamic phases?

We must say from the very beginning that there are not yet conclusive answers to these questions. The study of a possible relation between chaos and phase transitions is a very recent issue [26], and the results so far obtained and reported in the literature range from the claim of the discovery of a “universal” divergence in  $\lambda_1$  near criticality in a class of models describing clusters of particles [27], to the observation that the Lyapounov exponent attains its minimum in correspondence with the phase transition in Ising-like coupled map lattices [28], and to the apparent insensitivity to the liquid-solid phase transition of the Lyapounov spectra of hard-sphere and Lennard-Jones systems [29].

Our simulation results are plotted in Figs.4 and 5. The  $O(1)$  case has been studied more extensively than the others because of practical reasons of computational effort (for example single runs for the  $O(4)$  model usually required at least two weeks of CPU time on a fast HP 9000/735 computer).

The first numerical evidence is that in presence of a second order phase transition a rather sharp and “cuspy” transition between different behaviours of  $\lambda_1(T)$  is found at  $T_c$  (where the critical values  $T_c$  are those determined by means of Binder cumulants). Moreover, the qualitative behaviour of  $\lambda_1(T)$  appears very different in the thermodynamically ordered and disordered regions respectively. In fact, in the former region  $\lambda_1$  rapidly increases with  $T$ , whereas in the latter region  $\lambda_1(T)$  displays an almost flat pattern above  $T_c$  (note that  $\lambda_1(T)$  is expected to change again at very large  $T$  because the dynamics is asymptotically integrable in the limit  $T \rightarrow \infty$ ; this effect has been numerically checked at very high temperatures and

is clearly evident in Fig.4 —  $O(1)$  case — at  $T/T_c \sim 10^4$ ). This suggests that the phase transition has a dynamical counterpart in a passage from a weakly to a strongly chaotic regime.

It is remarkable that the shape of  $\lambda_1(T)$  is significantly different in presence or in absence of a second order phase transition. In fact, in the case of one dimensional lattices with short range interactions — where no phase transition is present —  $\lambda_1(T)$  has a very smooth pattern (see Ref. [8]). This fact has been checked more specifically for the  $\varphi^4$  model by computing  $\lambda_1(T)$  for the  $O(2)$  symmetry case on a two-dimensional lattice; as a consequence of the Mermin-Wagner theorem, here a second order phase transition is forbidden and in fact this model undergoes an infinite order phase transition (Kosterlitz-Thouless-Berezinsky). The shape of  $\lambda_1(T)$  again displays a major change so that the low and high temperature regimes are very different. However the transition between these two regimes is now smooth [30].

It is worth to emphasize that the average of a *local* property of microscopic dynamics — the average instability measured by  $\lambda_1$  — is sensitive to a *collective* phenomenon like a second order phase transition.

It could be argued that in the critical region almost any “honest” observable will show a peculiar behaviour and that this reflects the tendency of the statistical measure to become singular at the transition point, regardless of the ensemble chosen. In the framework of equilibrium statistical mechanics this is certainly true, because Gibbs measure is the fundamental mathematical object upon which everything relies. In the thermodynamic limit also the microcanonical measure, which is the invariant measure of the microscopic Hamiltonian dynamics, will have to become singular. However the microcanonical measure is not the ultimate mathematical entity that can be considered, so that the Hamiltonian dynamics approach gives meaning to the question of the possible existence of a *more fundamental* phenomenon at the very ground of a phase transition.

Lyapounov exponents provide the necessary link to such unexplored land. The details on this point are given in the next Section, where we recall how the geometrization of Hamiltonian dynamics proceeds in the language of Riemannian geometry, and how average



geometric properties of some suitable manifold directly influence the average dynamical instability quantified by  $\lambda_1$ .

### III. GEOMETRY OF DYNAMICS AND THE PHASE TRANSITION

Let us here sketch the main points of the Riemannian theory of chaos in physical systems, details can be found in ref.s [3–8].

#### A. Riemannian geometrization of newtonian dynamics

The trajectories of a dynamical system described by the Lagrangian function

$$L(\mathbf{q}, \dot{\mathbf{q}}) = \frac{1}{2} a_{ik}(\mathbf{q}) \dot{q}^i \dot{q}^k - V(\mathbf{q}) \quad (22)$$

are geodesics of the configuration space endowed with a proper Riemannian manifold structure described by the metric tensor

$$g_{ik}(\mathbf{q}) = 2[E - V(\mathbf{q})] a_{ik}(\mathbf{q}) . \quad (23)$$

This metric is known as Jacobi metric and is defined in the region of the configuration space where  $E > V(\mathbf{q})$ . In local coordinates, the geodesic equations on a Riemannian manifold are given by

$$\frac{d^2 q^i}{ds^2} + \Gamma_{jk}^i \frac{dq^j}{ds} \frac{dq^k}{ds} = 0 \quad (24)$$

where  $s$  is the proper time and  $\Gamma_{jk}^i$  are the Christoffel coefficients of the Levi-Civita connection associated with  $g_{ik}$ , i.e.  $\Gamma_{jk}^i = \frac{1}{2W} \delta^{im} (\partial_j W \delta_{km} + \partial_k W \delta_{mj} - \partial_m W \delta_{jk})$ , where  $W = E - V(\mathbf{q})$ ; proper time and physical time are related by  $ds^2 = 2W^2 dt^2$ . By direct computation, using  $g_{ik} = (E - V(\mathbf{q})) \delta_{ik}$ , it can be easily verified that the geodesic equations yield

$$\frac{d^2 q^i}{dt^2} = - \frac{\partial V}{\partial q^i} \quad (25)$$

i.e. Newton's equations associated with the Lagrangian (22). These equations can be also derived as geodesics of a manifold consisting of an enlarged configuration spacetime  $M \times \mathbb{R}^2$ , with local coordinates  $(q^0, q^1, \dots, q^i, \dots, q^N, q^{N+1})$ . To such purpose this space is endowed with a non-degenerate pseudo-Riemannian metric, first introduced by Eisenhart [31], whose arc-length is

$$ds^2 = g_{\mu\nu} dq^\mu dq^\nu = a_{ij} dq^i dq^j - 2V(\mathbf{q})(dq^0)^2 + 2 dq^0 dq^{N+1} , \quad (26)$$

called *Eisenhart metric*. The natural motions are obtained as the canonical projection of the geodesics of  $(M \times \mathbb{R}^2, g_E)$  on the configuration space-time,  $\pi : M \times \mathbb{R}^2 \mapsto M \times \mathbb{R}$ . Within the totality of geodesics only those whose arclength is positive-definite and is given by  $ds^2 = c_1^2 dt^2$  correspond to natural motions, what is equivalent to requiring the condition  $q^{N+1} = \frac{1}{2}c_1^2 t + c_2^2 - \int_0^t L d\tau$  for the extra-coordinate  $q^{N+1}$  [3,4];  $c_1$  and  $c_2$  are real arbitrary constants.

## B. Curvature and instability of geodesic motions

There is an important relation between the curvature of a manifold and the stability of its geodesics. It is described by the Jacobi – Levi-Civita (JLC) equation for the *geodesic separation vector field*  $J(s)$ .

The evolution of  $J$  contains the whole information on the stability — or instability — of a given reference geodesic  $\gamma(s)$ : in fact if  $|J|$  grows exponentially then the geodesic will be unstable in the Lyapounov sense, otherwise it will be stable. It is remarkable that such an evolution is completely determined by the Riemann curvature tensor  $R_{jkl}^i$  according to the JLC equation

$$\frac{\nabla^2 J^i}{ds^2} + R_{jkl}^i \frac{dq^j}{ds} J^k \frac{dq^l}{ds} = 0 , \quad (27)$$

where  $\frac{\nabla}{ds}$  is the covariant derivative.

In the large  $N$  case, under suitable hypotheses [7,8], it is possible to derive a scalar effective stability equation. Briefly, among the others, the main assumptions are: *i*) that

the ambient manifold is *almost-isotropic*, this essentially means that – after some suitable coarse-graining – the ambient manifold would look like a constant curvature manifold; *ii*) that the curvature felt along an unstable geodesic can be reasonably modeled by a gaussian stochastic process. The final result is [8]

$$\frac{d^2\psi}{ds^2} + \langle k_R \rangle_\mu \psi + \langle \delta^2 k_R \rangle_\mu^{1/2} \eta(s) \psi = 0 , \quad (28)$$

where  $\psi$  denotes any of the components of  $J$  in Eq. (27) because now all of them obey the same effective equation of motion;  $\langle k_R \rangle_\mu = \frac{1}{N} \langle K_R \rangle_\mu$  where  $K_R$  is the Ricci curvature of the ambient manifold:  $K_R = R_{ik} \dot{q}^i \dot{q}^k$  and  $R_{ik} = R_{ijk}^j$ ;  $\langle \cdot \rangle_\mu$  stands for microcanonical average, and  $\langle \delta^2 k_R \rangle_\mu$  is a shorthand for  $\frac{1}{N-1} \langle \delta^2 K_R \rangle_\mu$ , the mean square fluctuation of the Ricci curvature;  $\eta(s)$  is a gaussian  $\delta$ -correlated random process of zero mean and unit variance.

Equation (28) is a scalar equation which, *independently of the knowledge of dynamics*, provides a measure of the average degree of instability of the dynamics through the growth-rate of  $\psi(s)$ . The peculiar properties of a given Hamiltonian system enter Eq. (28) through the global geometric properties  $\langle k_R \rangle_\mu$  and  $\langle \delta^2 k_R \rangle_\mu$  of the ambient Riemannian manifold. Moreover  $\langle k_R \rangle_\mu$  and  $\langle \delta^2 k_R \rangle_\mu$  are functions of the energy  $E$  of the system — and of the energy density  $\varepsilon = E/N$  as well, which is the relevant quantity at  $N \rightarrow \infty$  — so that from (28) we can obtain the energy dependence of the geometric instability exponent.

Equation (28) is of the form

$$\frac{d^2\psi}{ds^2} + \Omega(s) \psi = 0 \quad (29)$$

representing a stochastic oscillator where the squared frequency  $\Omega(s)$  is a stochastic process; the derivation of this equation does not depend on a particular choice of the metric. For Hamiltonian systems with a diagonal kinetic energy matrix, i.e.  $a_{ij} = \delta_{ij}$ , by choosing as ambient manifold for the geometrization of dynamics the enlarged configuration space-time equipped with Eisenhart metric (26), it is found that the only non-vanishing component of the Ricci tensor is  $R_{00} = \Delta V$ , thus Ricci curvature is a function of the coordinates  $q^i$  only and one has  $k_R(q) = \Delta V/N$ . Using  $dt^2 = ds^2$ , the stochastic oscillator equation (29) can be written

$$\frac{d^2\psi}{dt^2} + \Omega(t) \psi = 0 , \quad (30)$$

where mean and variance of  $\Omega(t)$  are given by

$$\Omega_0 = \langle k_R \rangle_\mu = \frac{1}{N} \langle \Delta V \rangle_\mu , \quad (31)$$

$$\sigma_\Omega^2 = \langle \delta^2 k_R \rangle_\mu = \frac{1}{N} \left( \langle (\Delta V)^2 \rangle_\mu - \langle \Delta V \rangle_\mu^2 \right) . \quad (32)$$

The process  $\Omega(t)$  is specified by  $\Omega_0$ ,  $\sigma_\Omega^2$  and its time correlation function  $\Gamma_\Omega(t_1, t_2)$ . We consider a stationary and  $\delta$ -correlated process  $\Omega(t)$  with  $\Gamma_\Omega(t_1, t_2) = \tau \sigma_\Omega^2 \delta(|t_2 - t_1|)$ , where  $\tau$  is a characteristic time scale of the process. At present the evaluation of this time scale is still a rather delicate point, where some arbitrariness enters the theory. In Ref. [8] these two time scales are defined by

$$\tau_1 = \left\langle \frac{dt}{ds} \right\rangle \frac{\pi}{2\sqrt{\Omega_0 + \sigma_\Omega}} , \quad \tau_2 = \left\langle \frac{dt}{ds} \right\rangle \frac{\Omega_0^{1/2}}{\sigma_\Omega} , \quad (33)$$

that are combined to give  $\tau$  as follows

$$\tau^{-1} = 2 (\tau_1^{-1} + \tau_2^{-1}) . \quad (34)$$

As we shall see below, at low temperatures this formula seems to predict a satisfactory temperature-dependence of  $\tau$ , in fact, by adjusting a constant factor that multiplies  $\tau_1$ , the theoretical prediction of  $\lambda_1(T)$  is in very good agreement with numerical computations. At high temperatures we have to take care of the fact that  $\Omega_0$  and  $\sigma_\Omega$  are both increasing functions of  $T$ , even though the system approaches an integrable limit.

Whenever  $\Omega(t)$  in Eq. (30) has a non-vanishing stochastic component, the solution  $\psi(t)$  is exponentially growing on the average [32]. Our estimate for the (largest) Lyapounov exponent is then given by the growth-rate of  $\|(\psi, \dot{\psi})(t)\|^2$  according to the definition

$$\lambda_1 = \lim_{t \rightarrow \infty} \frac{1}{2t} \log \frac{\psi^2(t) + \dot{\psi}^2(t)}{\psi^2(0) + \dot{\psi}^2(0)} . \quad (35)$$

The ratio  $(\psi^2(t) + \dot{\psi}^2(t))/(\psi^2(0) + \dot{\psi}^2(0))$  is computed by means of a technique developed by Van Kampen, summarized in Ref. [8], that yields

$$\lambda_1(\Omega_0, \sigma_\Omega, \tau) = \frac{1}{2} \left( \Lambda - \frac{4\Omega_0}{3\Lambda} \right) ,$$

$$\Lambda = \left( 2\sigma_\Omega^2 \tau + \sqrt{\left( \frac{4\Omega_0}{3} \right)^3 + (2\sigma_\Omega^2 \tau)^2} \right)^{1/3} . \quad (36)$$

The quantities  $\Omega_0$ ,  $\sigma_\Omega$  and  $\tau$  can be computed as static, i.e., *microcanonical* averages. Therefore Eq. (36) gives an analytic, though approximate, formula for the largest Lyapounov exponent independently of the numerical integration of the dynamics and of the tangent dynamics.

### C. Geometric signatures of the phase transition

As already noted above, on the one hand the largest Lyapounov exponent is sensitive to the phase transition, on the other hand, in the Riemannian description of chaos,  $\lambda_1$  is intimately related to the average curvature properties of the “mechanical manifolds”. These quantities are computed as integrals on manifolds just like other statistical quantities of thermodynamic kind. This means that by means of statistical-mechanical-like computations we can obtain non-trivial informations about dynamics. Hence the following questions: is there any peculiarity in the geometric properties associated with the dynamics of systems which — as statistical systems in thermal equilibrium — exhibit a phase transition? And in particular, do the curvature fluctuations show any noticeable behaviour in correspondence with the phase transition itself?

#### 1. Results of the computations

Let us now report on the results of the the computation of the geometric properties of the “mechanical” manifolds sampled by the numerical geodesics.

For the  $\varphi^4$  models, the Ricci curvature per degree of freedom along a geodesic of  $(M \times \mathbb{R}^2, g_E)$  is given by

$$k_R = \frac{1}{Nn} \sum_{\alpha=1}^n \sum_{\mathbf{i}} \frac{\partial^2 V}{\partial (\varphi_{\mathbf{i}}^{\alpha})^2} = 2Jd - m^2 + \lambda \frac{n+2}{Nn} \sum_{\alpha=1}^n \sum_{\mathbf{i}} (\varphi_{\mathbf{i}}^{\alpha})^2. \quad (37)$$

High and low temperature behaviours of this quantity can be easily derived. In the limit  $T \rightarrow 0$  we can replace, at any site  $\mathbf{i}$  of the lattice,  $\|\varphi_{\mathbf{i}}^{\alpha}\|^2 = \sum_{\alpha=1}^n (\varphi_{\mathbf{i}}^{\alpha})^2$  with the constant value  $\varphi_0^2 = m^2/\lambda$ ; this value is obtained by minimizing the potential part of the Hamiltonian (5). Hence, for a generic  $O(n)$  case, we have

$$\lim_{T \rightarrow 0} k_R = \frac{2}{n} (Jdn + m^2) \quad (38)$$

and with the values we chose for the constants —  $J = 1$ ,  $m^2 = 2$ ,  $d = 3$ ,  $\lambda = 0.1$  — it is  $k_R = 10$  in the  $O(1)$  case,  $k_R = 8$  in the  $O(2)$  case, and  $k_R = 7$  in the  $O(4)$  case respectively. These values perfectly check with our numerical findings as is shown by Fig.6 where  $\kappa(T) = (\langle k_R \rangle_t(T) - 2Jd) / (\langle k_R \rangle_t(T=0) - 2Jd)$  is synoptically displayed for all the models; the average  $\langle \cdot \rangle_t$  is defined in Eq. (10). At low temperature  $\langle k_R \rangle_t(T)$  only slightly deviates from its limiting zero-temperature value, as is shown by Fig.7; this fact is intuitively interpreted as a sign of a weakly chaotic dynamics.

Also in the opposite limit,  $T \rightarrow \infty$ , these systems are again integrable. In fact at increasing temperature the variables  $\varphi_{\mathbf{i}}^{\alpha}$  become larger and larger so that the Hamiltonian (5) describes a collection of quartic oscillators that are less and less perturbed by the quadratic coupling term. In this limit the canonical partition function is factored in terms of functions of the following form

$$\int_0^{\infty} dx x^{\nu} e^{-ax^{\alpha}} = \frac{1}{\alpha} \Gamma\left(\frac{\nu+1}{\alpha}\right) a^{-(\nu+1)/\alpha}, \quad (39)$$

with  $\nu = 0$ , and where  $\Gamma(x)$  is the Euler gamma. Hence the canonical average of any even power  $\nu$  of the field is

$$\langle (\varphi_{\mathbf{i}}^{\alpha})^{\nu} \rangle = \left(\frac{\beta\lambda}{4}\right)^{-\frac{\nu}{4}} \frac{\Gamma\left(\frac{\nu+1}{4}\right)}{\Gamma\left(\frac{1}{4}\right)} \quad (40)$$

and vanishes for any odd power  $\nu$ .

From Eqs.(37) and (40) we find a canonical estimate of  $\langle k_R \rangle_{\mu}$  which differs from the microcanonical one by  $\mathcal{O}(\frac{1}{N})$  terms

$$\langle k_R \rangle_\mu \sim 2Jd - m^2 + \frac{2(n+2)\Gamma(\frac{3}{4})\sqrt{\lambda}}{\Gamma(\frac{1}{4})}\sqrt{T} + \mathcal{O}(\frac{1}{N}) . \quad (41)$$

This prediction is compared to the numerically computed values of  $\langle k_R \rangle_t(T)$  in Fig.7; at very high temperature the agreement is very good.

In order to compute the average curvature fluctuations,  $\langle \delta^2 k_R \rangle_\mu$ , we first notice that

$$\langle \delta^2 k_R \rangle = \langle k_R^2 \rangle - \langle k_R \rangle^2 = \lambda^2 \left( \frac{n+2}{Nn} \right)^2 \left\{ \left\langle \left( \sum_{\mathbf{i}} \|\varphi_{\mathbf{i}}\|^2 \right)^2 \right\rangle - \left( \sum_{\mathbf{i}} \langle \|\varphi_{\mathbf{i}}\|^2 \rangle \right)^2 \right\} \quad (42)$$

and, as in the large  $T$  limit we consider all the  $\varphi_{\mathbf{i}}^\alpha$  decoupled, we find

$$\langle \delta^2 k_R \rangle = \lambda^2 (n+2)^2 \left\{ \langle (\varphi_{(\mathbf{i})}^\alpha)^4 \rangle - \langle (\varphi_{(\mathbf{i})}^\alpha)^2 \rangle^2 \right\} \quad (43)$$

where  $\varphi_{(\mathbf{i})}^\alpha$  denotes any representative of the now independent degrees of freedom. The Gibbsian, canonical, average in the  $T \rightarrow \infty$  limit is now easily found to be

$$\langle \delta^2 k_R \rangle^G \sim \left\{ \frac{\Gamma(5/4)}{\Gamma(1/4)} - \left[ \frac{\Gamma(3/4)}{\Gamma(1/4)} \right]^2 \right\} (n+2)^2 4\lambda T . \quad (44)$$

In order to compare the predictions of Eq. (44) with our numerical results, and also in order to use it in the analytic prediction of the Lyapounov exponent, we have to take into account the correction that relates canonical and microcanonical averages [32] that now reads

$$\langle \delta^2 k_R \rangle_\mu = \langle \delta^2 k_R \rangle^G - \frac{\beta^2}{C_V} \left( \frac{\partial \langle k_R \rangle}{\partial \beta} \right)^2 . \quad (45)$$

The high temperature partition function  $Z$  is obtained by raising to the  $Nn$ -th power the integral  $\int d\varphi \exp[-\beta(\lambda/4)\varphi^4] \sim \beta^{-1/4}$ . Then, using  $F = -(1/Nn\beta) \ln Z$  and  $C_V = -T(\partial^2 F / \partial T^2)$ , we find  $c_V \rightarrow 1/4$ . By the way, this is in very good agreement with our numerical results for the high temperature values of  $c_V$ ; this is somehow less clear in the  $O(4)$  case because  $c_V$  was computed only in the transition region. From Eqs. (45) and (44) we can now obtain the final result

$$\langle \delta^2 k_R \rangle_\mu \sim \left\{ \frac{\Gamma(5/4)}{\Gamma(1/4)} - 2 \left[ \frac{\Gamma(3/4)}{\Gamma(1/4)} \right]^2 \right\} (n+2)^2 4\lambda T . \quad (46)$$

In Fig.8 we report the temperature dependence of the time average of the Ricci curvature fluctuations,  $\sigma_\Omega(T) \equiv \langle \delta^2 k_R \rangle_t$ . In Fig.9 we also give a comparison of  $\sigma_\Omega$  with the prediction of Eq.(46) for the  $O(1)$  model.

The common feature of the three models is that a cusp-like (singular) behaviour of the curvature fluctuations is observed in correspondence with the phase transition.

Moreover, curvature fluctuations display very smooth energy density dependence, or temperature dependence as well, in those systems where no finite order phase transition is present (see ref. [8]). In Fig.10 we report also  $\sigma_\Omega(T)$  in the case of 2-d  $\varphi^4$  model with  $O(2)$  symmetry; in this case a second order phase transition is forbidden and actually the system undergoes a Kosterlitz-Thouless phase transition. The cusp-like behaviour of curvature fluctuations has now disappeared and  $\sigma_\Omega(T)$  is a monotonically increasing function of  $T$ ; visibly, something still happens at the transition point ( $T_c \simeq 1.5$ ) so that this case appears to be “intermediate” between no phase transition at all and a second order phase transition. Similar results have been found for planar 2-d and 3-d classical Heisenberg models [30,33] and in a preliminary investigation of the dual (gauge) version of the Ising model in 3-d [34]: the cusp-like behaviour of the curvature fluctuations always shows up when a second order phase transition is present, and the singular point is located at the critical temperature, within the numerical accuracy.

In the light of the Riemannian description of Hamiltonian chaos given above, we understand why the temperature dependence of the largest Lyapounov exponent  $\lambda_1$  is so peculiar near and at the critical temperature (see Figs.4 and 5):  $\lambda_1(T)$  reflects the “cuspy” pattern of  $\sigma_\Omega(T)$  near  $T_c$ . In the next Subsection we make a conjecture about the deep meaning of these singular behaviours shown by  $\lambda_1(T)$  and  $\sigma_\Omega(T)$ .

As the invariant measure for an autonomous Hamiltonian flow is the microcanonical measure on the constant energy surfaces of phase space, our numerical computations of  $\langle k_R \rangle_t$  and of  $\langle \delta^2 k_R \rangle_t$  are good estimates of the quantities  $\Omega_0(T)$  and  $\sigma_\Omega(T)$ , i.e. microcanonical averages, that enter Eqs. (33) and (36). The analytic computation of  $\lambda_1(T)$  by means of these formulae yields an unsatisfactory result that overestimates  $\lambda_1(T)$  at low temperatures



(though the temperature dependence is correct) and that steeply increases at high temperatures instead of saturating (before decreasing again at extremely high  $T$ ). The high temperature result appears particularly bad, however this is only due to the asymptotic growth with  $T$  of both  $\langle k_R \rangle$  and  $\langle \delta^2 k_R \rangle$  — given by Eqs. (41) and (46) and confirmed numerically — which has no special meaning for dynamical instability. The estimate of the decorrelation time-scale of curvature fluctuations along the geodesics is still somehow rudimental in the above outlined Riemannian framework, therefore one expects that some improvement is needed on this point. As a matter of fact, it is possible to substantially improve the theoretical predictions by simply multiplying the decorrelation time scale  $\tau$  of Eq.(34) by a constant factor which is model dependent and different below and above  $T_c$ . Moreover, at high temperatures, in computing  $\tau_1$  and  $\tau_2$  given in Eq.(33), we have subtracted to  $\Omega_0(T)$  and  $\sigma_\Omega(T)$  their respective asymptotic behaviours given by Eqs. (41) and (46). The analytic predictions for  $\lambda_1(T)$  are now in very good agreement with numeric results with the exception of the critical region, where something is apparently still lacking. The results are reported in Figs.11, 12 and 13 where it is well evident that the best agreement between theory and numerical experiments is obtained in the  $O(1)$  case; a very good agreement is still present at low temperatures for the  $O(2)$  model and it becomes poorer in the  $O(4)$  model. The comparison at  $T > T_c$  suffers – in the cases of  $O(2)$  and  $O(4)$  – of a restricted range of temperature values (we focused our attention only to the transition region because of the already mentioned problems) where subtracting to  $\Omega_0(T)$  and  $\sigma_\Omega(T)$  their asymptotic values is less meaningful.

However it is not out of place to remind that the theoretical computation of Lyapounov exponents is not a routine task at all, and that the approach reported here is at present the only theoretical method available to cope with the computation of  $\lambda_1$ . What is important here is that with some simple and reasonable adjustment the above sketched analysis still applies and yields good results. Refinements of the geometrical theory of chaos are beyond the aim of the present work, rather we are interested in using it as it is at present to get a hold of the deep origin of the peculiarities of the dynamics at a phase transition.

### D. A topological conjecture

We shall now try to grasp the possible significance of the above reported cusp-like, thus possibly singular, behaviour of the curvature fluctuations at the transition point for the  $\varphi^4$  lattice systems. As a first step toward this goal, we shall try to reproduce such a peculiar behaviour of curvature fluctuations in abstract geometric models. A preliminary step in this direction was already presented in Ref. [30], applied to the case of planar spin models.

The choice of a geometric *toy model* stems from the following considerations. Weakly and strongly chaotic geodesic flows can “live” on homologically trivial manifolds, i.e., on manifolds that are diffeomorphic to an  $N$ -sphere, in other words, non-trivial topology is not necessary to make chaos, conversely, a sudden topological change in a family of manifolds can abruptly affect their geometric properties and the degree of chaoticity of geodesic flows. Therefore, let us consider — for instance — the two families of surfaces of revolution immersed in  $\mathbb{R}^3$  defined as follows:

$$\mathcal{F}_\varepsilon = (f_\varepsilon(u) \cos v, f_\varepsilon(u) \sin v, u) , \quad (47a)$$

$$\mathcal{G}_\varepsilon = (u \cos v, u \sin v, f_\varepsilon(u)) , \quad (47b)$$

where

$$f_\varepsilon(u) = \pm \sqrt{\varepsilon + u^2 - u^4} , \quad \varepsilon \in [\varepsilon_{\min}, +\infty) , \quad (48)$$

and  $\varepsilon_{\min} = -\frac{1}{4}$ . Some members of the two families are depicted in Fig. 14. In both cases there exists a critical value of the parameter  $\varepsilon$ ,  $\varepsilon_c = 0$ , corresponding to a change in the *topology* of the surfaces. In particular the manifolds  $\mathcal{F}_\varepsilon$  are diffeomorphic to a torus  $\mathbb{T}^2$  for  $\varepsilon < 0$  and to a sphere  $\mathbb{S}^2$  for  $\varepsilon > 0$ . In the other case, one has instead a change in the number of connected components: the manifolds  $\mathcal{G}_\varepsilon$  are diffeomorphic to *two* spheres for  $\varepsilon < 0$  and to one sphere for  $\varepsilon > 0$ . Computing the Euler-Poincaré characteristic  $\chi$  one finds  $\chi(\mathcal{F}_\varepsilon) = 0$  if  $\varepsilon < 0$ , and  $\chi(\mathcal{F}_\varepsilon) = 2$  otherwise, while  $\chi(\mathcal{G}_\varepsilon)$  equals either 4 or 2 when  $\varepsilon$  is respectively negative or positive. Let us now compute the  $\varepsilon$ -dependence of the average

curvature properties of these surfaces as  $\varepsilon \rightarrow \varepsilon_c$ . Let  $M$  belong to one of the two families under investigation. The gaussian curvature  $K$  is given by [35]

$$K = \frac{x'(x''y' - x'y'')}{y(x'^2 + y'^2)^2} \quad (49)$$

where the functions  $x(u)$  and  $y(u)$  represent the coefficients of the general form  $M(u, v) = (y(u) \cos v, y(u) \sin v, x(u))$  of parametrized surfaces of revolution, and the prime denotes differentiation with respect to  $u$ . Now the fluctuations of  $K$  are computed as follows

$$\sigma^2 = \langle K^2 \rangle - \langle K \rangle^2 = A^{-1} \int_M K^2 dS - \left( A^{-1} \int_M K dS \right)^2, \quad (50)$$

where  $A$  is the area of  $M$  and  $dS$  is the invariant surface element. Both families of surfaces, in spite of having very different curvature properties on the average<sup>2</sup>, exhibit a singular behaviour in the curvature fluctuation  $\sigma$  as  $\varepsilon \rightarrow \varepsilon_c$ , as shown in Fig. 15.

These results suggest — at a heuristic level — that, from the point of view of the geometric description of the dynamics, a phase transition might correspond to a *topology change* in the manifold underlying the motion. The relevance of topological concepts for the theory of phase transitions has been already emphasized (see Ref. [36]) though in a more abstract context. Here we suggest that topological aspects of phase transitions might also concern the manifolds that are “just behind” dynamics, and not only those deep mathematical objects that are involved in Ref. [36]. In our opinion this subject deserves further investigation to go beyond the heuristic level. In fact the study of dynamics and of its geometric and topologic counterparts could eventually lead to a better understanding of the nature of ergodicity breaking and thus of the very nature of phase transitions.

---

<sup>2</sup>For instance,  $\langle K \rangle(\varepsilon) = 0$  in the  $\mathcal{F}_\varepsilon$  case as  $\varepsilon < 0$ , while the same average curvature is positive and diverging as  $\varepsilon \rightarrow 0$  for  $\mathcal{G}_\varepsilon$ .

#### IV. CONCLUDING REMARKS

Let us now summarize the main points of the present work and comment about their meaning.

By studying some classical lattice  $\varphi^4$  models that undergo second order or Kosterlitz-Thouless phase transitions, it has been found that the natural microscopic dynamics — derived from the Hamiltonian functions of these systems — clearly reveals the presence of the phase transition. The invariant measure of Hamiltonian dynamics is the microcanonical measure, equivalent — in the thermodynamic limit — to the canonical measure which is sampled by usual MonteCarlo algorithms. Therefore one could argue that it is not surprising that Hamiltonian dynamics yields the same results of a MonteCarlo stochastic dynamics. As a matter of fact using Hamiltonian dynamics just to sample the microcanonical measure would not be so interesting, whereas the important point raised by the present work is that Hamiltonian dynamics brings about new observables and a new framework to tackle phase transitions. Mainly Lyapounov exponents are the new observables intrinsic to the dynamics, and the differential-geometric treatment of dynamical instability is the new framework.

As well as thermodynamic observables, dynamic and geometric observables are sensitive to a second order phase transition which can be recognized through their peculiar “non-smooth” behaviours. The common wisdom on phase transitions suggests that non-smooth behaviours of any observable are expected near the transition point, as a consequence of the tendency of the measure to become singular at  $T = T_c$  in the limit  $N \rightarrow \infty$ . In the light of our results we suggest that a deeper explanation might be possible: a major topological change of the “mechanical” manifolds could be the common root of the peculiar behaviours of both dynamic and thermodynamic observables in presence of a phase transition. Here topology is meant in the sense of the De Rham’s cohomology.

On a purely phenomenological ground it might be surprising that the largest Lyapounov exponent, which measures an average *local* property of the dynamics, is sensitive to a *collective*, and therefore global, phenomenon like a phase transition. In fluids, for example,

it is well evident that molecular chaos has nothing to do with the macroscopic patterns of the velocity field. It is even possible to have chaotic motions of fluid droplets (Lagrangian chaos) in presence of regular Eulerian velocity fields (i.e. in laboratory reference frame).

However, within the Riemannian framework outlined in the preceding Sections, Lyapounov exponents appear tightly related to the geometry of the “mechanical” manifolds, and geometry dramatically changes in presence of a major change of topology. Thus our topological conjecture seems to naturally account for this – at first sight counterintuitive – sensitivity of the largest Lyapounov exponent to a macroscopic collective phenomenon.

It is worth mentioning here that, at the best of our knowledge, there is only another framework where Lyapounov exponents can be, at least in principle, analytically computed. This is a field-theoretic framework, already mentioned in the Introduction [13–15], based on a path-integral formulation of classical mechanics, where Lyapounov exponents are seen as expectation values of suitable operators. There are many interesting points in this framework that could probably reveal a fertile relationship with the Riemannian geometric approach which is behind our present work. Let us mention some of them: ergodicity breaking, which - as we discussed in the Introduction - is a more general concept than symmetry breaking, in the field-theoretic context appears related to a supersymmetry breaking, moreover this supersymmetry breaking can occur also at finite  $N$  [13]; Lyapounov exponents turn out related to mathematical objects that have many analogies with definitions and concepts of the de Rham’s cohomology theory [15] what might be useful in future investigations about the relation between Lyapounov exponents and topology at a phase transition.

In conclusion we believe that the dynamic approach, besides the conceptual aspects mentioned above, could contribute to complement the standard approaches of statistical mechanics to the description of phase transitions, and it might hopefully be particularly helpful in those cases where these standard methods may encounter some difficulty, as is the case of disordered and frustrated systems, polymers in the continuum, lattice gauge theories where no symmetry-breaking transition occurs.

## ACKNOWLEDGMENTS

We thank S. Caracciolo, E. G. D. Cohen, R. Livi, and M. Rasetti for many fruitful discussions. This work has been carried out under the EC program Human Capital and Mobility, contract N° UE ERBCHRXCT940579 and N° OFES 950200.

## REFERENCES

- <sup>a</sup> During the editing of this paper Lando Caiani tragically died.
- <sup>b</sup> Present address: INFN, unità del Politecnico di Torino, Corso Duca degli Abruzzi 24, I-10129 Torino, Italy. Electronic address: lapo@polito.it
- <sup>c</sup> Also at INFN, unità di Trieste, Italy. Electronic address: clementi@sissa.it
- <sup>d</sup> Also at INFN, sezione di Firenze, Italy. Electronic address: pettini@fi.infn.it
- <sup>e</sup> Also at INFN, sezione di Firenze, and INFN, unità di Firenze, Italy. Electronic address: pettini@arcetri.astro.it
- <sup>f</sup> Electronic address: gatto@sc2a.unige.ch
- [1] N. S. Krylov, *Works on the foundations of statistical mechanics* (Princeton University Press, Princeton, NJ, 1979).
- [2] M.C.Gutzwiller, J. Math. Phys. **18**, 806 (1977); J.F.C. van Velsen, J.Phys. A: Math. Gen. **13**,833 (1980); G.K. Savvidy, Nucl. Phys. B**246**, 302 (1984); A. Knauf, Comm. Math. Phys. **110**, 89 (1987).
- [3] M. Pettini, Phys. Rev. E **47**, 828 (1993).
- [4] L. Casetti and M. Pettini, Phys. Rev. E **48**, 2340 (1993);
- [5] M. Cerruti-Sola and M. Pettini, Phys. Rev. E **51**, 53 (1995), and Phys. Rev. E **53**, 179 (1996).
- [6] M. Pettini and R. Valdettaro, Chaos **5**, 646 (1995).
- [7] L. Casetti, R. Livi, and M. Pettini, Phys. Rev. Lett. **74**, 375 (1995).
- [8] L. Casetti, C. Clementi, and M. Pettini, Phys. Rev. E **54**, 5969 (1996).
- [9] N. Goldenfeld, *Lectures on phase transitions and the renormalisation group* (Addison-Wesley, New York, 1992).

- [10] G. Parisi, *Statistical field theory* (Addison-Wesley, New York, 1988).
- [11] J. Zinn-Justin, *Quantum and statistical field theory* (Oxford University Press, Oxford, 1989).
- [12] C.N. Yang, T.D. Lee, Phys. Rev. **87**, 404 (1952).
- [13] E. Gozzi and M. Reuter, Phys. Lett. B **233**, 383 (1989).
- [14] E. Gozzi, M. Reuter and W.D. Thacker, Chaos, Solitons & Fractals **2**, 441 (1992).
- [15] E. Gozzi and M. Reuter, Chaos, Solitons & Fractals **4**, 1117 (1994).
- [16] An early attempt in this direction can be found in: P. Butera and G. Caravati, Phys. Rev. A **36**, 962 (1987), for the planar XY model; see also Ref. [29].
- [17] L. Casetti, Physica Scripta **51**, 29 (1995).
- [18] H. Goldstein, *Classical mechanics*, (Addison-Wesley, Reading MA, 1980).
- [19] J. Lebowitz, J. Percus, and L. Verlet, Phys. Rev. **153**, 250 (1967).
- [20] *Monte Carlo and Molecular Dynamics of Condensed Matter Systems*, proceedings of the Euroconference and Summer School held in Villa Olmo, Como, July 1995, edited by K. Binder and G. Ciccotti (Editrice Compositori, Bologna, 1996).
- [21] B. Dunweg, in Ref. [20].
- [22] K. Binder, Z. Phys. B**43**, 119 (1981).
- [23] A. P. Young, in Ref. [20].
- [24] M. Pettini and M. Landolfi, Phys. Rev. A **41**, 768 (1990).
- [25] M. Pettini and M. Cerruti-Sola, Phys. Rev. A **44**, 975 (1991).
- [26] A first thorough attempt to relate Hamiltonian dynamics with phase transitions – in a mean-field model – can be found in: M. Antoni and S. Ruffo, Phys. Rev E **52**, 2361



- (1995).
- [27] A. Bonasera, V. Latora, A. Rapisarda, Phys. Rev. Lett. **75**, 3434 (1995).
  - [28] C.S. O'Hern, D.A. Egolf, H.S. Greenside, Phys. Rev. E **53**, 3374 (1996).
  - [29] Ch. Dellago, H.A. Posch, W.G. Hoover, Phys. Rev. E **53**, 1485 (1996); Ch. Dellago, H.A. Posch, Physica A **230**, 364 (1996).
  - [30] L. Caiani, L. Casetti, C. Clementi, and M. Pettini, Phys. Rev. Lett. **79**, 4361 (1997).
  - [31] L. P. Eisenhart, Ann. Math. **30**, 591 (1929).
  - [32] N. G. Van Kampen, Phys. Rep. **24**, 71 (1976).
  - [33] C. Clementi, Laurea thesis, University of Florence, Italy (1995).
  - [34] C. Clementi, unpublished.
  - [35] M. Spivak, *A comprehensive introduction to differential geometry* (Publish or Perish, Berkeley, CA, 1979), Vol. III.
  - [36] M. Rasetti, *Topological concepts in the theory of phase transitions*, in *Differential geometric methods in mathematical physics*, C. Döbner, ed. (Springer-Verlag, New York, NY, 1990); M. Rasetti, *Structural Stability in Statistical Mechanics*, in Springer Tracts in Mathematics, W. Güttinger Ed., Berlin, 1979.

## FIGURES

FIG. 1. Binder cumulants  $g(N, \varepsilon)$  *vs* energy density  $\varepsilon$  at different values  $N$  of the lattice sites. *a)* the  $O(1)$  case; *b)* the  $O(2)$  case; *c)* the  $O(4)$  case. Open circles refer to  $N = 4 \times 4 \times 4$ , full triangles refer to  $N = 6 \times 6 \times 6$ , and full circles refer to  $N = 8 \times 8 \times 8$ .

FIG. 2. Temperature  $T$  (twice the average kinetic energy per particle) is plotted *vs* energy density  $\varepsilon$ . Results of the  $O(1)$ ,  $O(2)$  and  $O(4)$  models are represented by full circles, open circles and open triangles respectively. Temperatures and energy densities of each model are scaled by the corresponding critical values obtained by means of Binder cumulants. The dashed line is a guide to the eye. Lattice size:  $N = 8 \times 8 \times 8$

FIG. 3. Specific heat per degree of freedom *vs* scaled temperature  $T/T_c$ .  $c_V = C_V/Nn$  and  $C_V$  is computed according to Eq.(19). Symbols: full circles for  $O(1)$ ; open circles for  $O(2)$  and open triangles for  $O(4)$ . Lattice size:  $N = 8 \times 8 \times 8$ .

FIG. 4. The largest Lyapounov exponent  $\lambda_1$  is plotted *vs* temperature for the  $O(1)$  model. A “non-smooth” feature at  $T = T_c$  is well evident. Lattice size:  $N = 8 \times 8 \times 8$ .

FIG. 5. Synopsis of  $\lambda_1(T)$  obtained for the  $O(1)$  model (full circles), for the  $O(2)$  model (open circles) and for the  $O(4)$  model (open triangles). Lattice size:  $N = 8 \times 8 \times 8$ .

FIG. 6. Reduced average Ricci curvature  $\kappa = (\langle k_R \rangle - 2Jd) / (\langle k_R(T=0) \rangle - 2Jd)$  *vs*  $T/T_c$ . Ricci curvature is so reduced in order to facilitate the comparison between the different models. Symbols: full circles for  $O(1)$ ; open circles for  $O(2)$  and open triangles for  $O(4)$ . Lattice size:  $N = 8 \times 8 \times 8$ .

FIG. 7.  $O(1)$  model. The average Ricci curvature  $\langle k_R \rangle$  is plotted *vs*  $T$  for a wide temperature range. The dashed horizontal line represents the integrable limit behaviour of  $\langle k_R \rangle(T)$  predicted by Eq.(38) and actually attained at low temperature by the average Ricci curvature computed for the  $O(1)$  model according to Eq.(37). Solid line represents the high temperature asymptotic behaviour of  $\langle k_R \rangle(T)$  predicted by Eq.(41), again pertaining an integrable limiting behaviour of the model.

FIG. 8. Average Ricci curvature fluctuations  $\sigma_\Omega$  vs  $T/T_c$ . The “cuspy” behaviour is well evident at  $T \simeq T_c$ . From top to bottom:  $O(4)$ ,  $O(2)$  and  $O(1)$  results. The cusp appear to soften at increasing dimension  $n$  of the symmetry group  $O(n)$ .

FIG. 9. Average Ricci curvature fluctuations  $\sigma_\Omega$  vs  $T$  for the  $O(1)$  model reported for a wide range of temperature. Solid line represents the high temperature asymptotic value given by Eq.(46).

FIG. 10. Average Ricci curvature fluctuations  $\sigma_\Omega$  vs temperature for the  $O(2)$  model on a square lattice ( $d = 2$ ) of  $N = 30 \times 30$  sites. The cusp is now absent and  $\sigma_\Omega(T)$  is a monotonously increasing function. Around  $T \simeq 1.5$ , on the basis of the temperature behaviour of other observables, the system is supposed to undergo a Kosterlitz-Thouless phase transition and, correspondingly, we can observe a change in the shape of  $\sigma_\Omega(T)$ . Here  $J = 1$ ,  $\lambda = 4$  and  $m^2 = 10$ .

FIG. 11. The numerical largest Lyapounov exponent  $\lambda_1$  (open circles) is plotted vs  $T$  for the  $O(1)$  model and is compared to the analytic prediction of Eq.(36) (full circles). The vertical solid line marks the transition temperature. The correlation time scale  $\tau$  is given by Eq.(34);  $\tau$  is rescaled by a constant factor equal to 0.65 at  $T < T_c$ , and by a factor 1.1 at  $T > T_c$ .

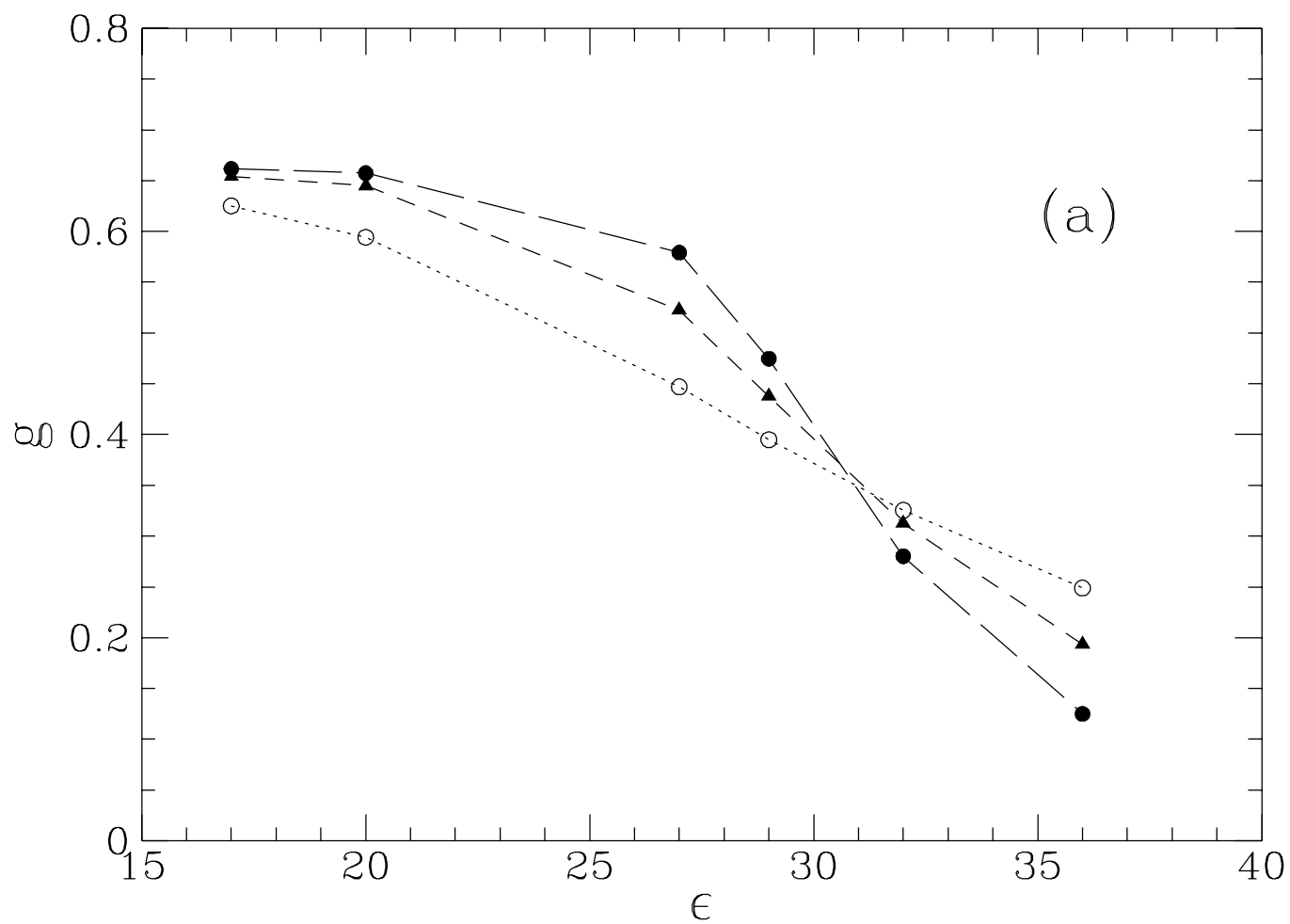
FIG. 12. The numerical largest Lyapounov exponent  $\lambda_1$  (open circles) is plotted vs  $T$  for the  $O(2)$  model and is compared to the analytic prediction of Eq.(36) (full circles). The vertical dashed line marks the transition temperature. Here  $\tau$  is rescaled by a constant factor equal to 3 at  $T < T_c$ , and by a factor 0.7 at  $T > T_c$ .

FIG. 13. The numerical largest Lyapounov exponent  $\lambda_1$  (open circles) is plotted vs  $T$  for the  $O(4)$  model and is compared to the analytic prediction of Eq.(36) (full circles). The vertical solid line marks the transition temperature. Here  $\tau$  is rescaled by a constant factor equal to 5.5 at  $T < T_c$ , and by a factor 0.6 at  $T > T_c$ .

FIG. 14. Some representatives of the two families of surfaces  $\mathcal{F}_\epsilon$  and  $\mathcal{G}_\epsilon$  defined in Eqs.(47a) and (47b) respectively. Each family is divided into two subfamilies by the critical surface corresponding to  $\epsilon_c = 0$  (middle members in the picture). Members of the same subfamily are diffeomorphic, whereas the two subfamilies are not diffeomorphic between them.

FIG. 15. The second moment of the gaussian curvature of the surfaces  $\mathcal{F}_\epsilon$  and  $\mathcal{G}_\epsilon$  is plotted *vs*  $\epsilon$ .  $\sigma$  is defined in Eq.(50),  $\epsilon$  is shifted by  $\epsilon_{min} = 0.25$  (see text) for graphical reasons. (a) refers to  $\mathcal{G}_\epsilon$  and (b) refers to  $\mathcal{F}_\epsilon$ . The cusps appear at  $\epsilon = 0$  where the topological transition takes place.

Fig. 1a



Caiani,Casetti,Clementi,Pettini,Pettini,Gatto  
“Geometry of dynamics and phase transitions...”

Fig. 1b

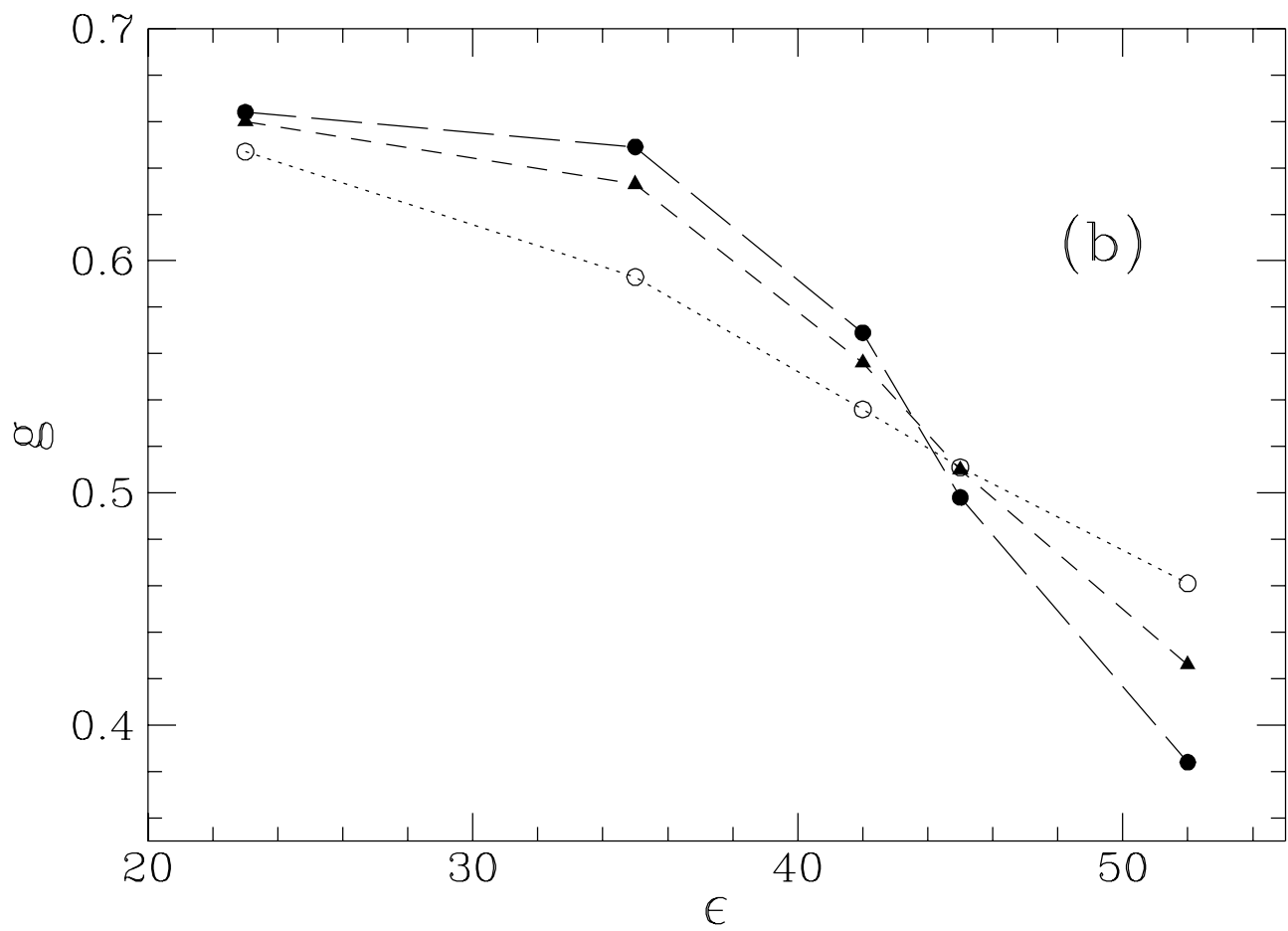
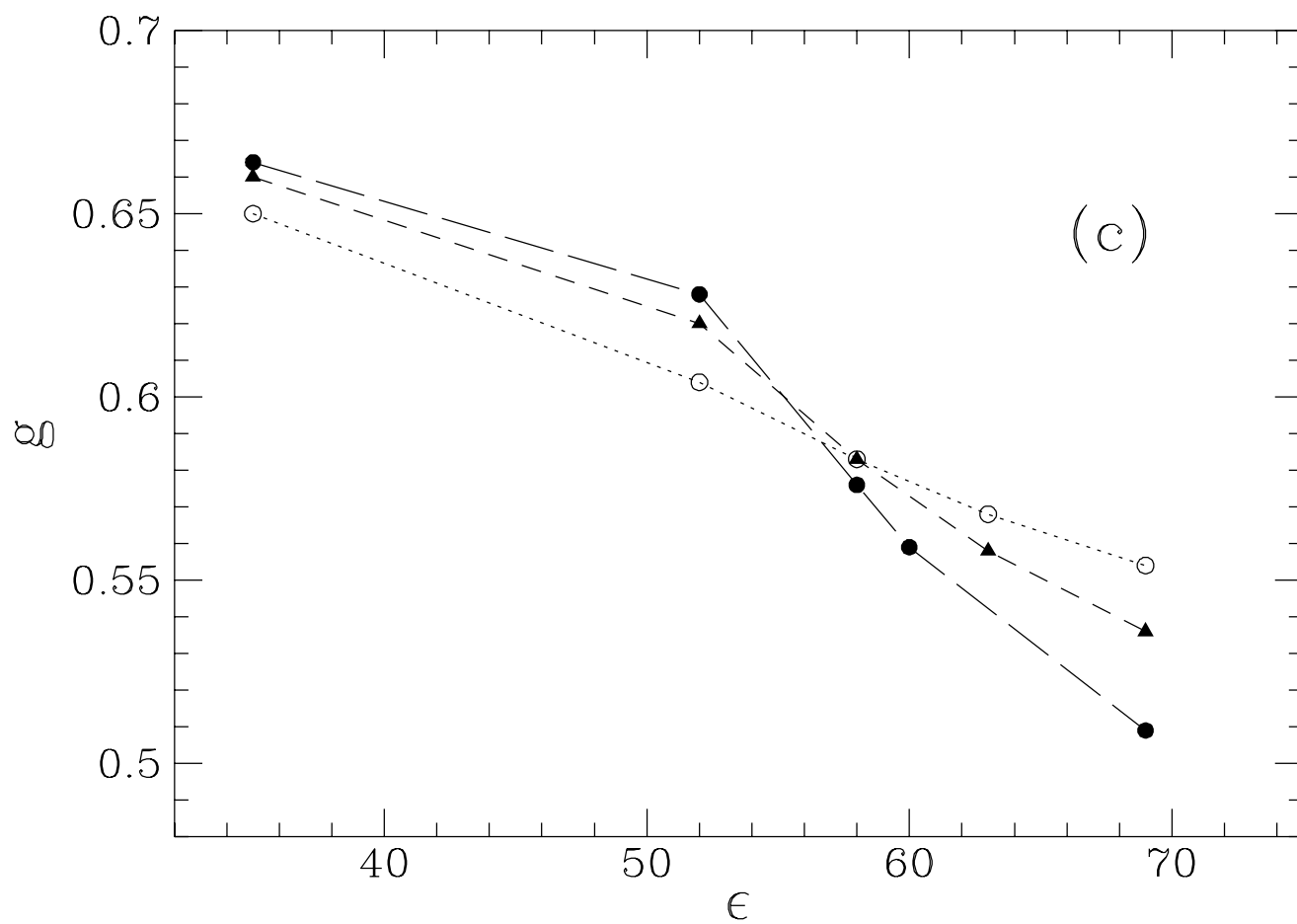


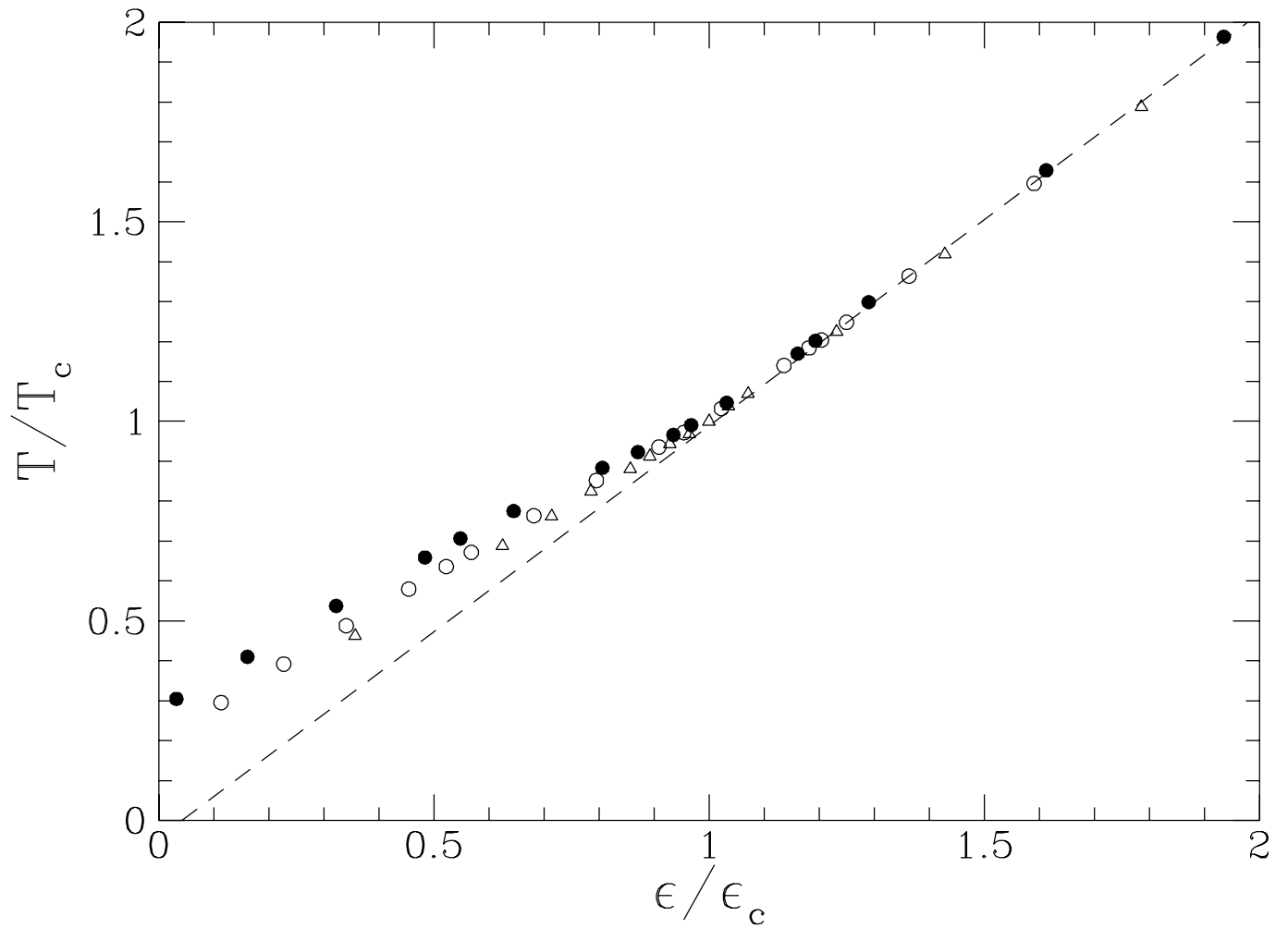
Fig. 1c



Caiani,Casetti,Clementi,Pettini,Pettini,Gatto

“Geometry of dynamics and phase transitions...”

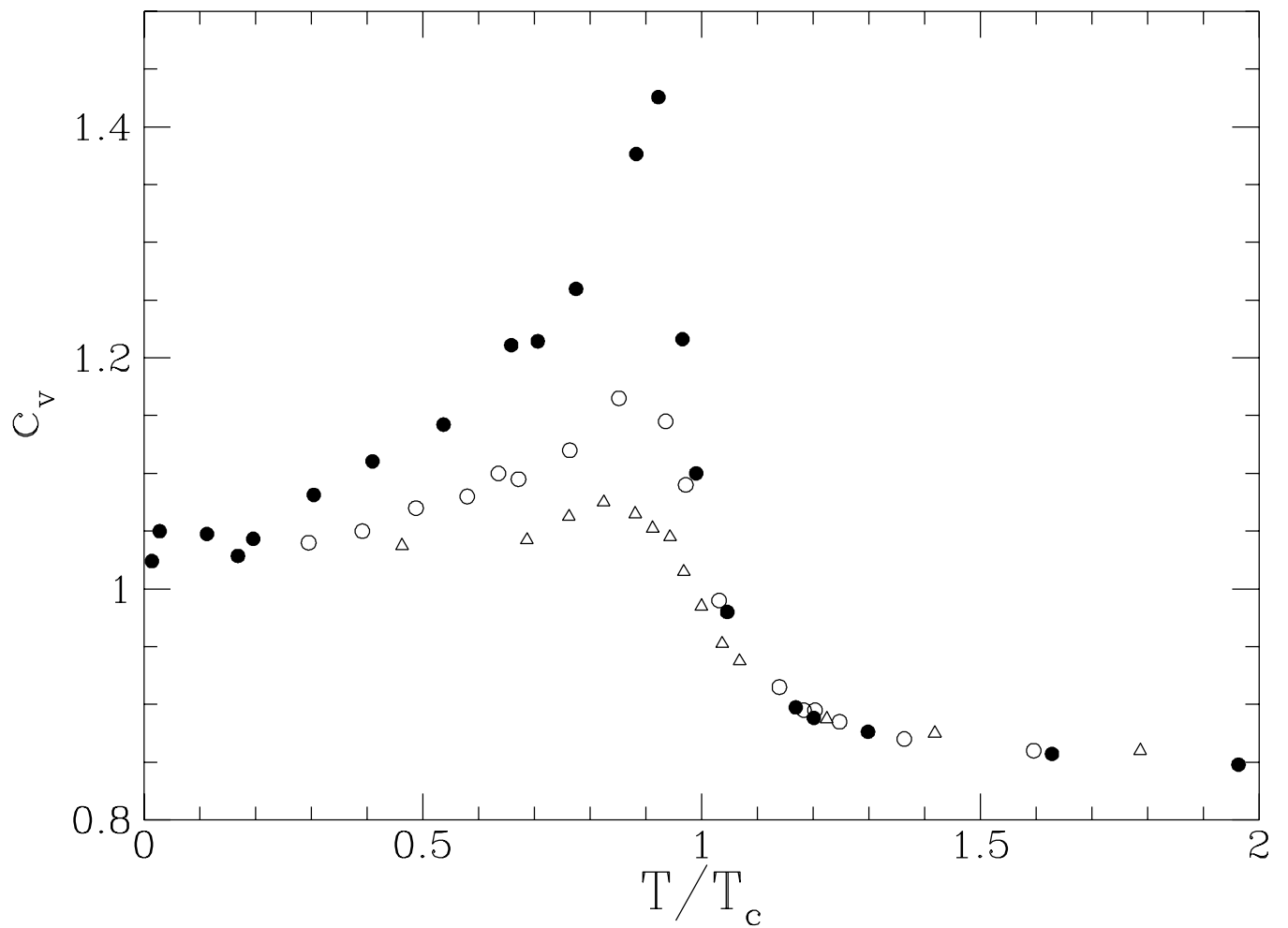
Fig. 2





Caiani,Casetti,Clementi,Pettini,Pettini,Gatto  
“Geometry of dynamics and phase transitions...”

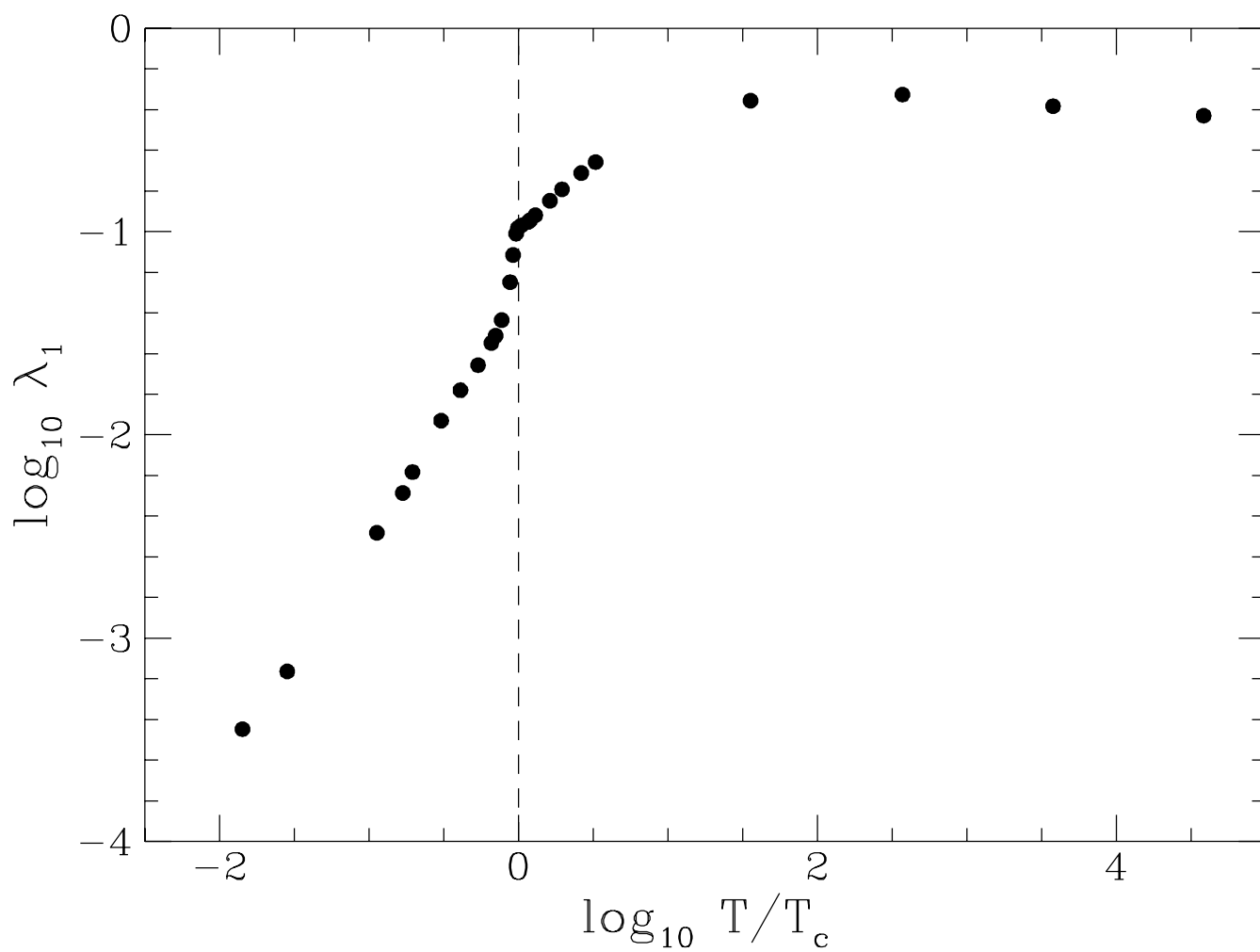
Fig. 3



Caiani,Casetti,Clementi,Pettini,Pettini,Gatto

“Geometry of dynamics and phase transitions...”

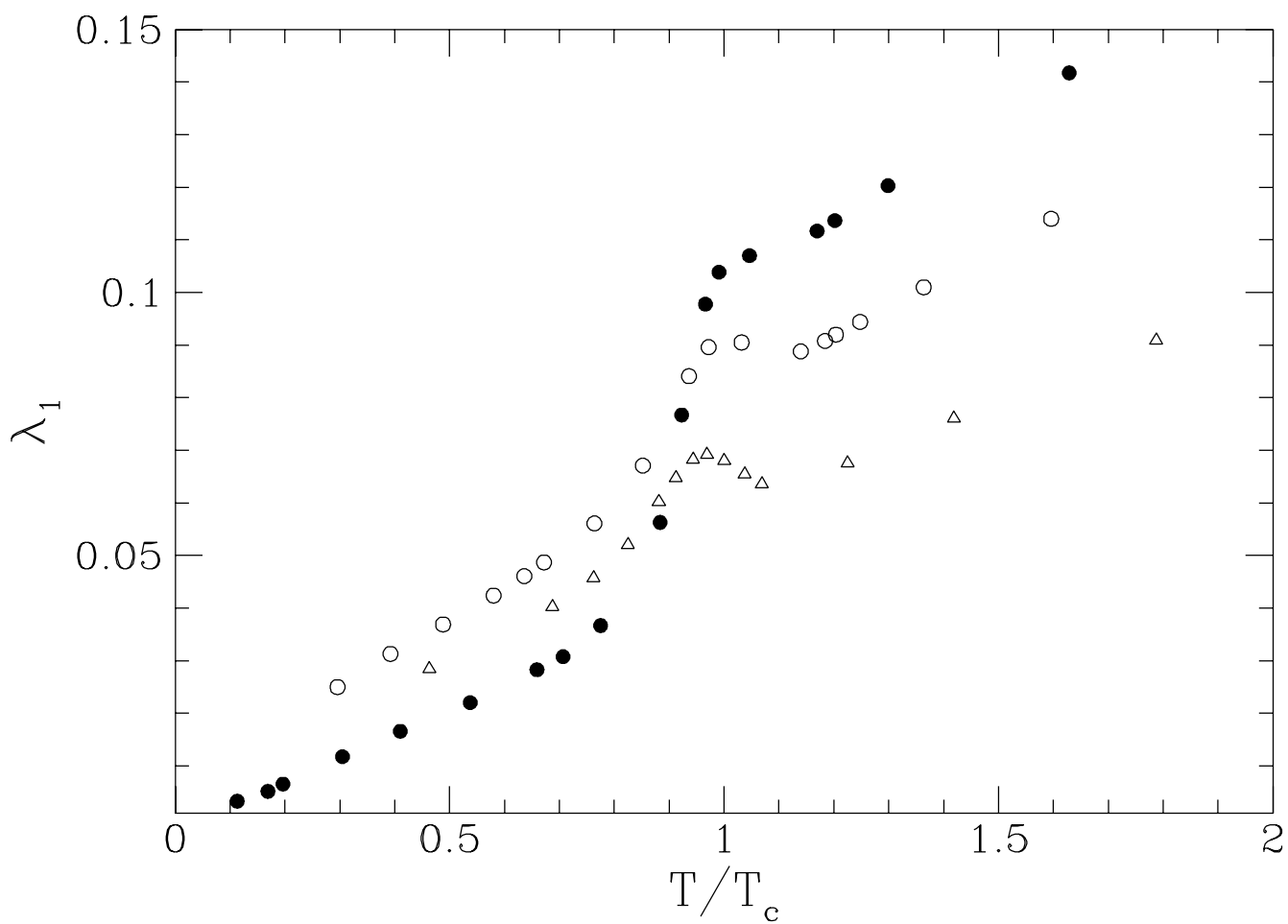
Fig. 4



Caiani,Casetti,Clementi,Pettini,Pettini,Gatto

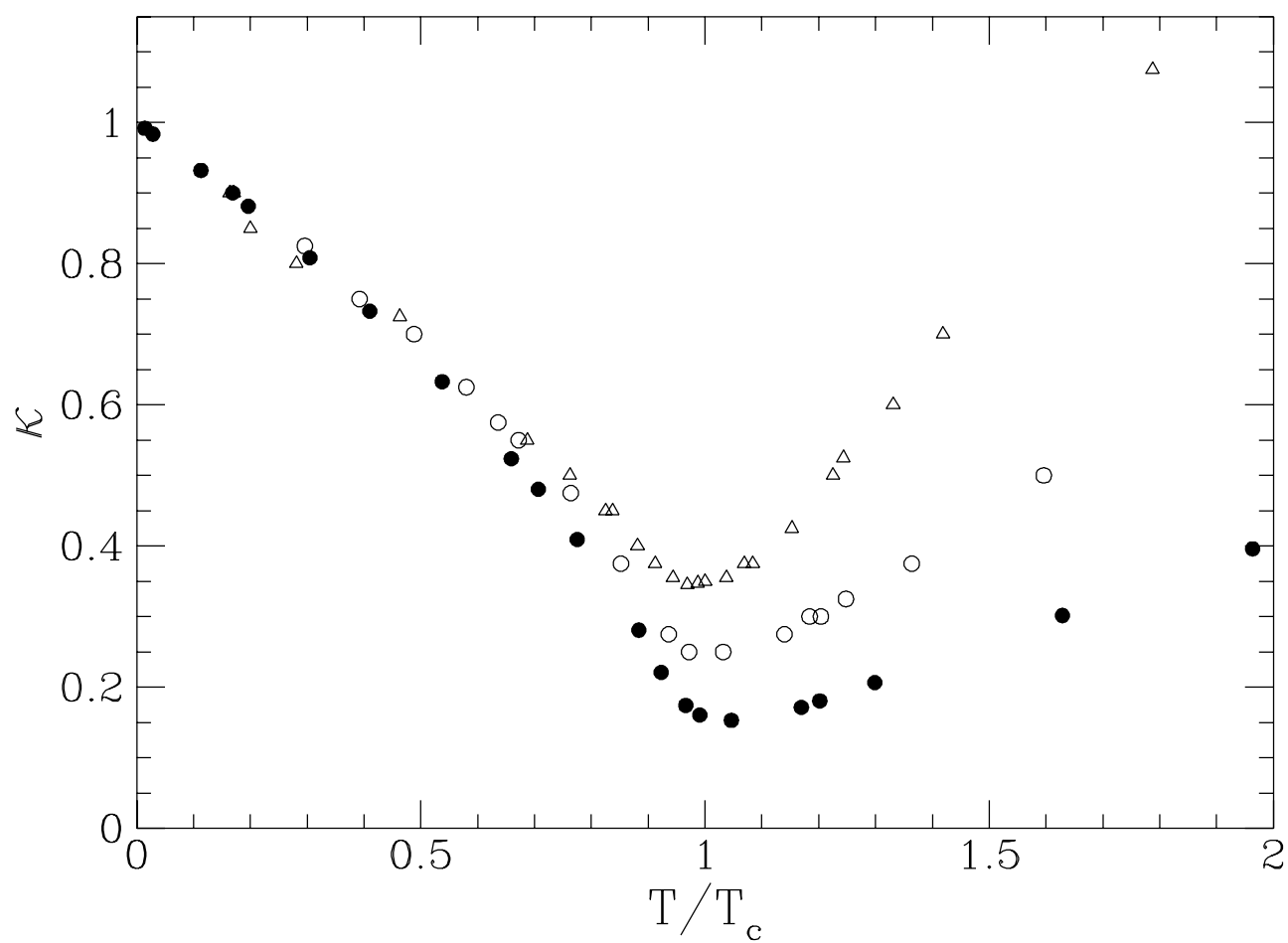
“Geometry of dynamics and phase transitions...”

Fig. 5



Caiani,Casetti,Clementi,Pettini,Pettini,Gatto  
“Geometry of dynamics and phase transitions...”

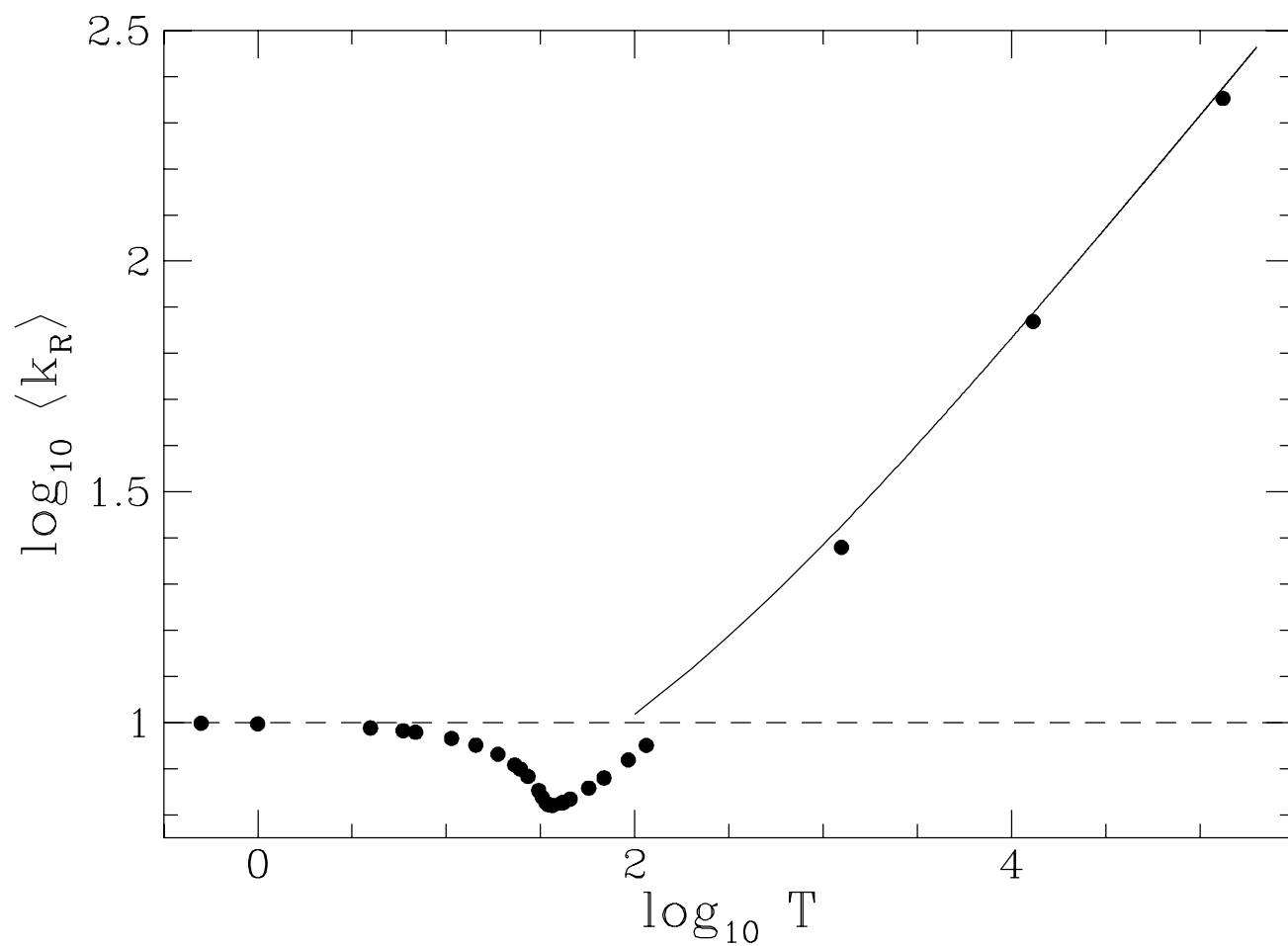
Fig. 6



Caiani,Casetti,Clementi,Pettini,Pettini,Gatto

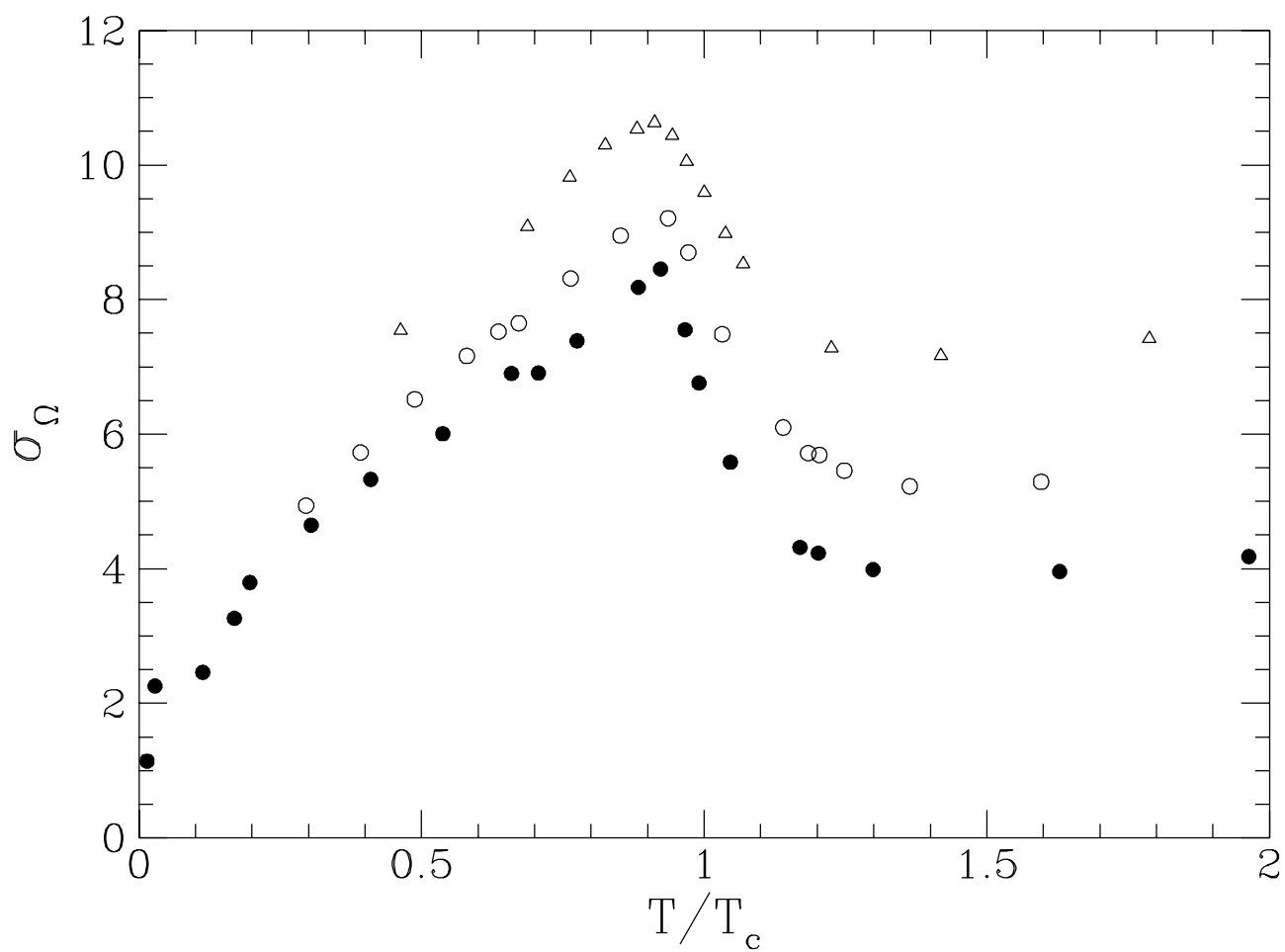
“Geometry of dynamics and phase transitions...”

Fig. 7



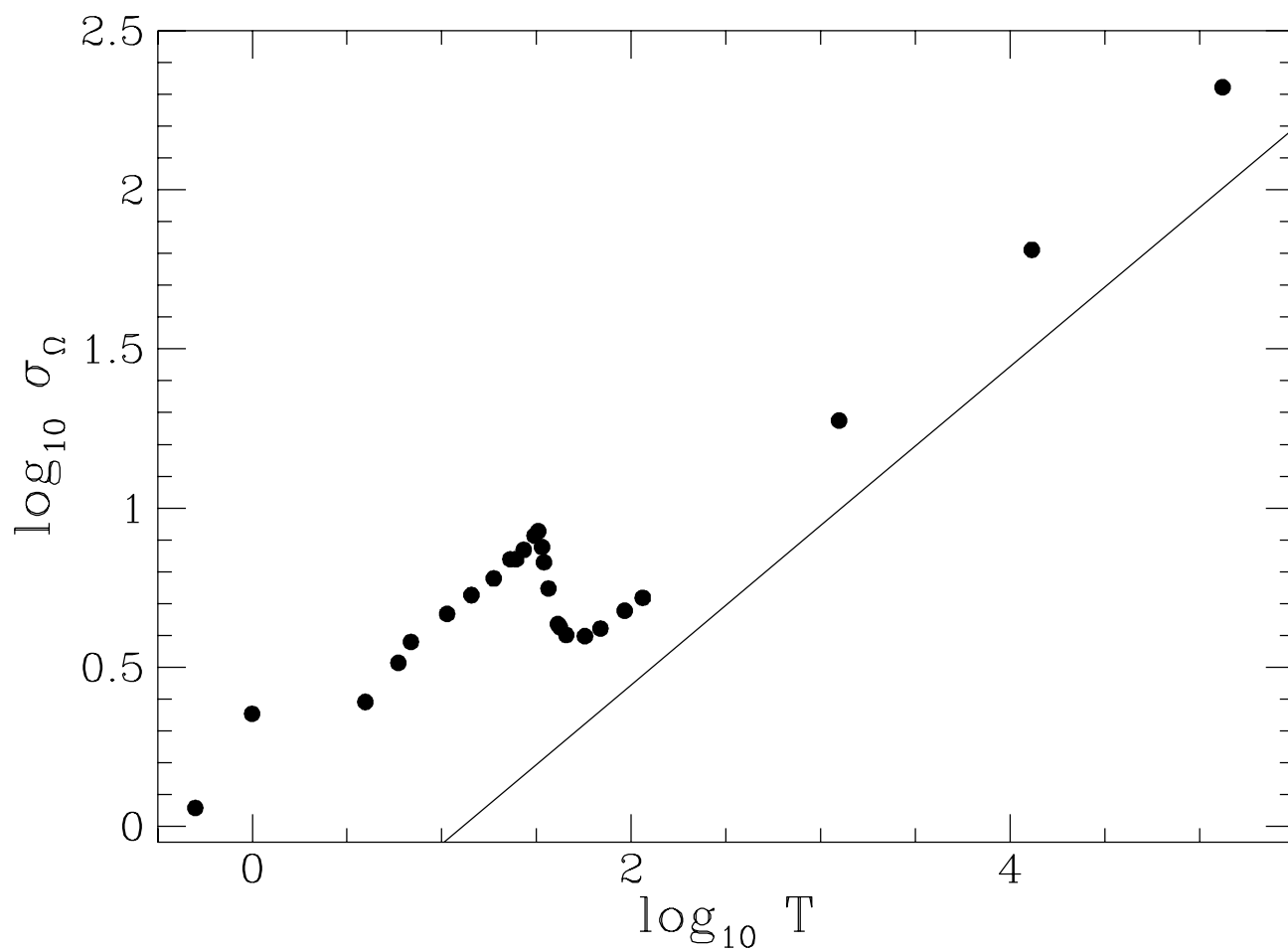
Caiani,Casetti,Clementi,Pettini,Pettini,Gatto  
“Geometry of dynamics and phase transitions...”

Fig. 8



Caiani,Casetti,Clementi,Pettini,Pettini,Gatto  
“Geometry of dynamics and phase transitions...”

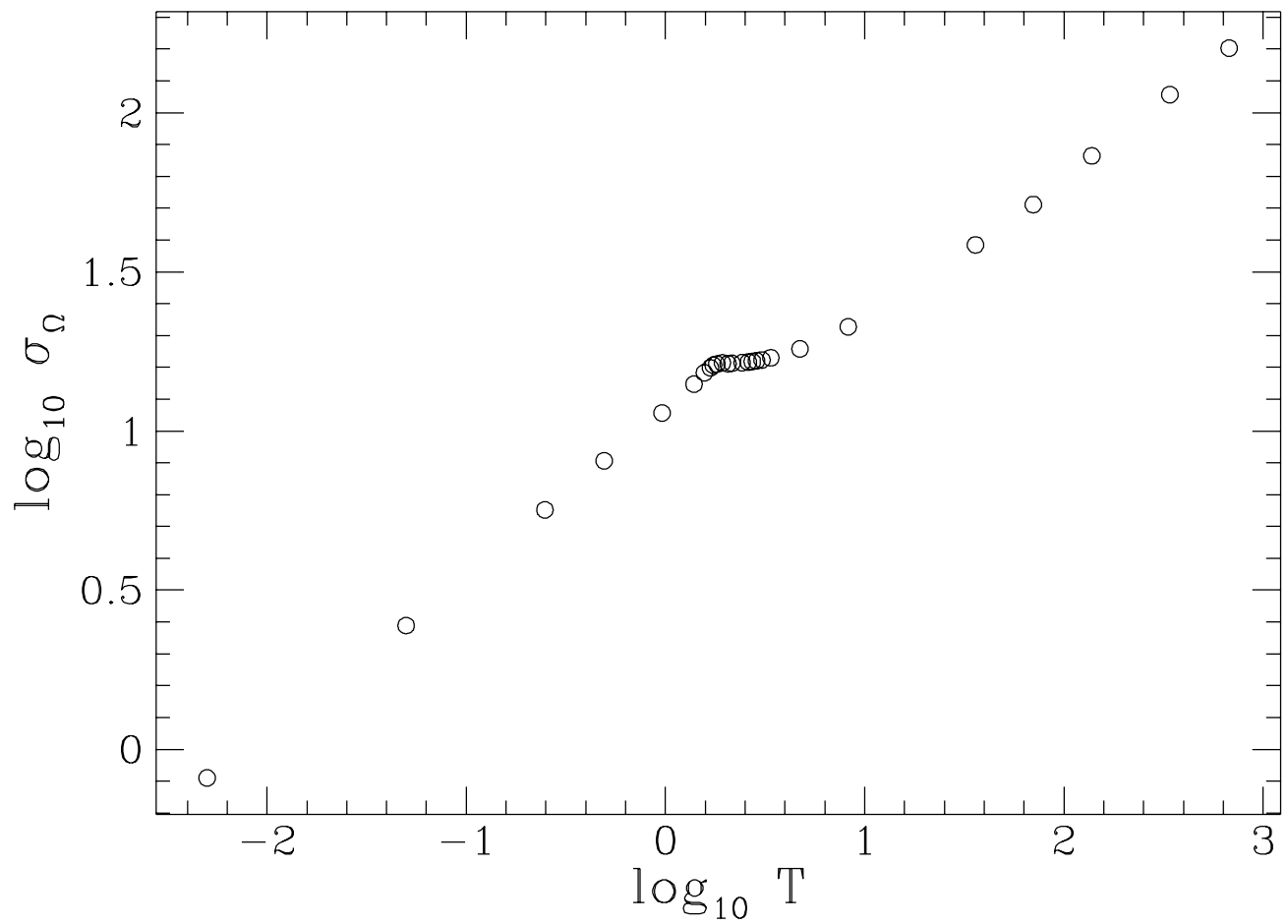
Fig. 9



Caiani,Casetti,Clementi,Pettini,Pettini,Gatto

“Geometry of dynamics and phase transitions...”

Fig. 10





Caiani,Casetti,Clementi,Pettini,Pettini,Gatto  
“Geometry of dynamics and phase transitions...”

Fig. 11

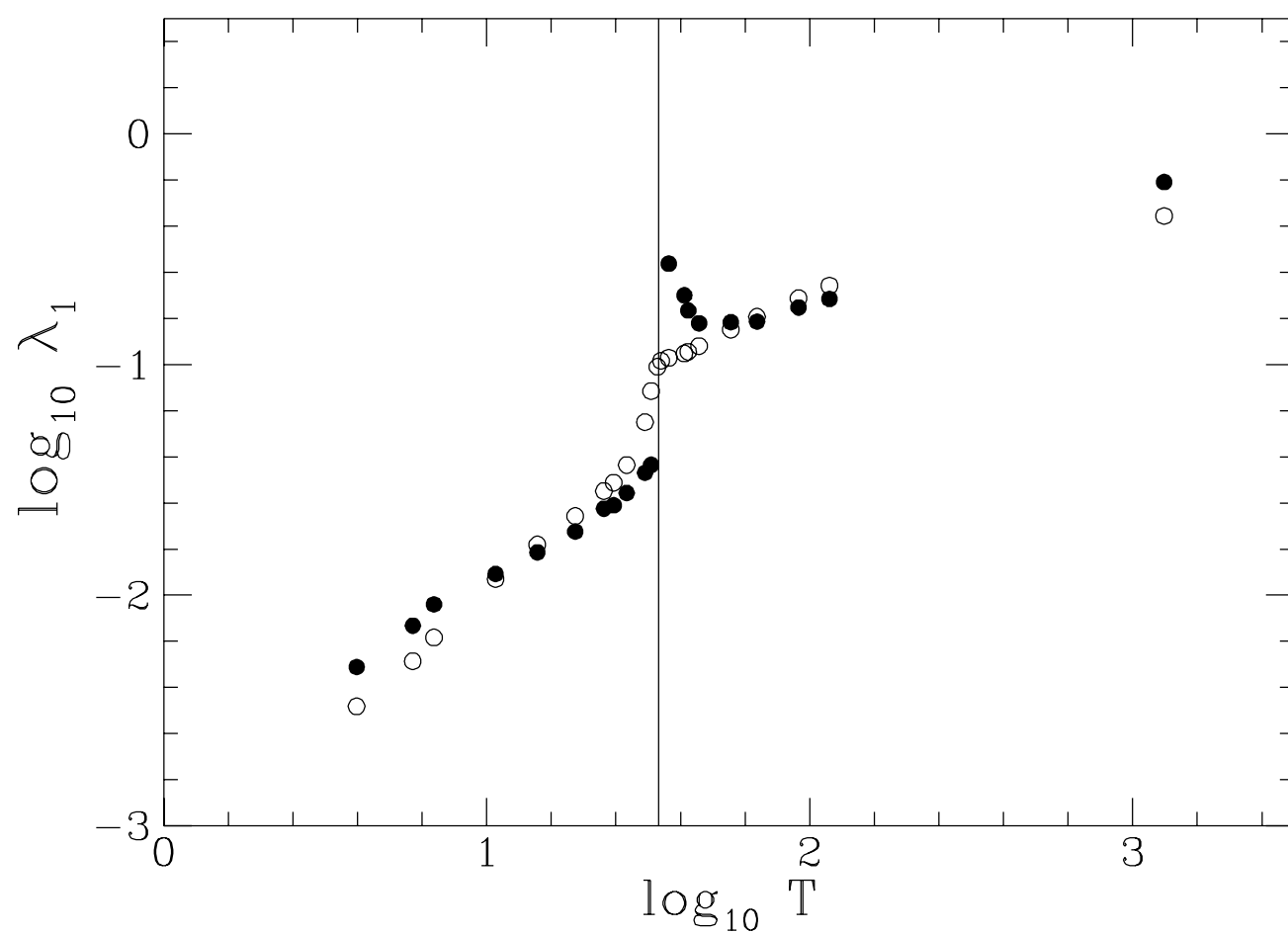
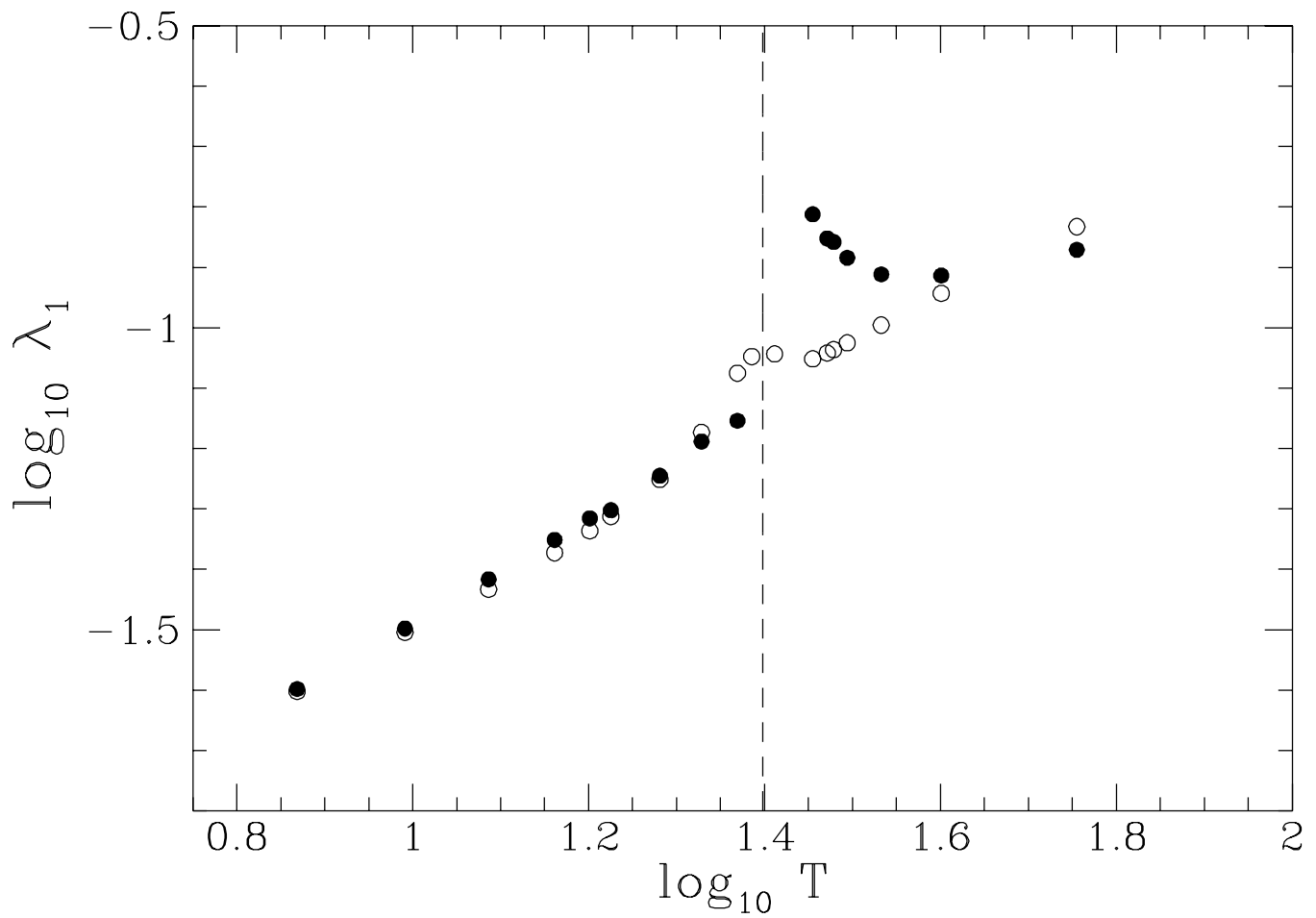


Fig. 12



Caiani,Casetti,Clementi,Pettini,Pettini,Gatto  
“Geometry of dynamics and phase transitions...”

Fig. 13

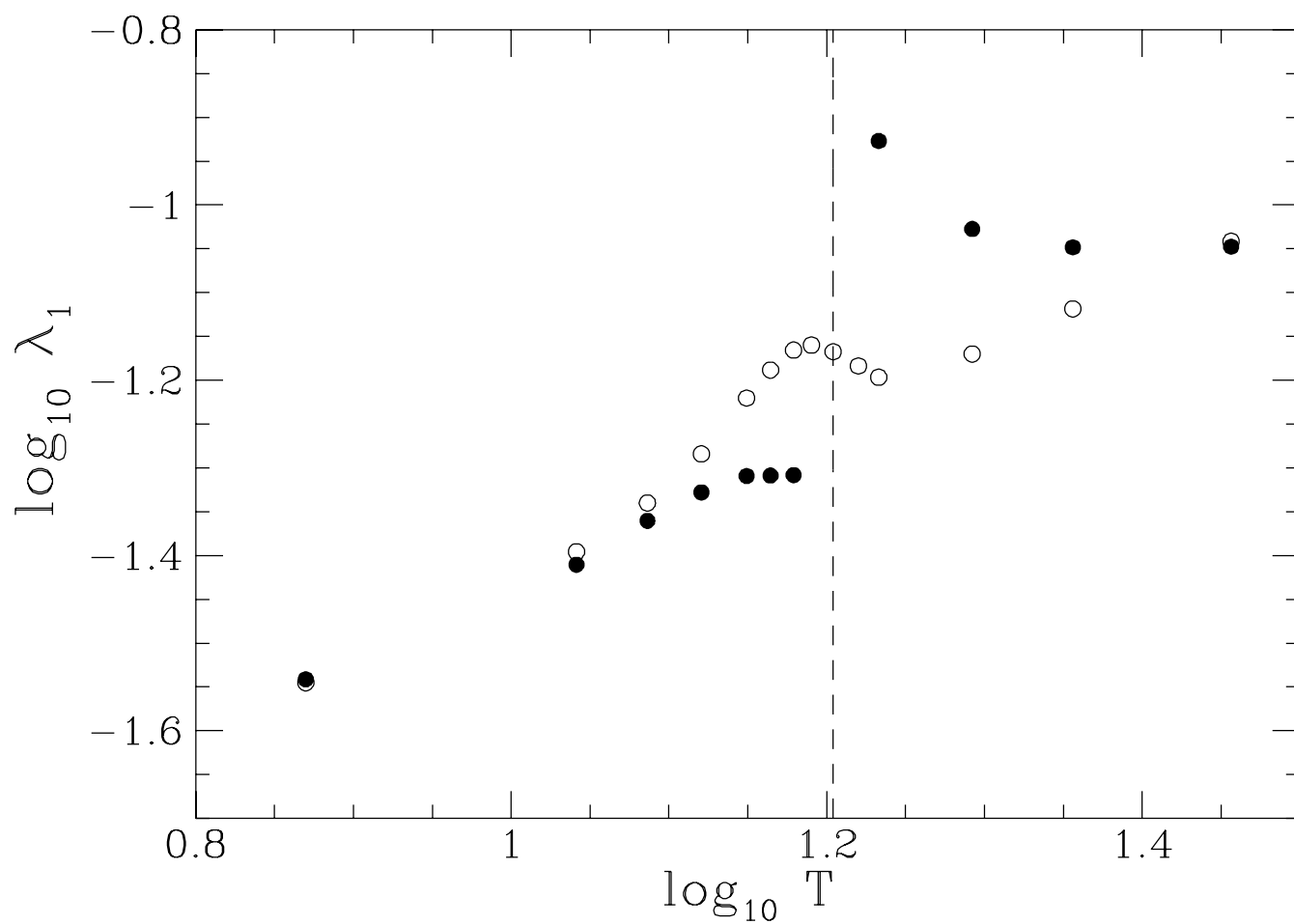




Fig. 15

